6-3-2016

The Effects of Ion Substitution on Perovskite Film Degradation in Controlled Humidity Environments

Eric David Grulke
eric.grulke@uconn.edu

The Effects of Ion Substitution on Perovskite Film Degradation in Controlled Humidity Environments

Eric David Grulke

B.S., University of Connecticut, 2014

A Thesis

Submitted in Partial Fulfillment of the

Requirements for the Degree of

Master of Science

At the

University of Connecticut

2016

APPROVAL PAGE

Masters of Science Thesis

The Effects of Ion Substitution on Perovskite Film Degradation in Controlled Humidity Environments

Presented by

Eric David Grulke, B.S.

Major Advisor_____

Alexander Agrios

Associate Advisor _____

Baikun Li

Associate Advisor _____

Prabhakar Singh

University of Connecticut

2016

A Special Thank You To

Dr. Alex Agrios

Dr. Baikun Li

Dr. Prabhakar Singh

Bowen Yang

Daniel Denyer and Yahya Alyami

Dave Kriz and Dr. Steve Suib

Table of Contents

Abstract

The demand for clean, renewable energy grows constantly as time progresses and harvesting solar energy has been identified as one of the key pieces in solving this puzzle. Through ambipolar diffusion and high absorption characteristics, perovskite based solar cells have seen a large jump in device efficiency over a short amount of time. Perovskite cells are also appealing due to their low cost and ease of manufacturing, with the potential of competing with silicon based solar cells in the future. However, stability issues due to environmental factors, such as reactivity to atmospheric moisture, have plagued perovskites. These issues often lead to the deterioration of the material and a corresponding loss of efficiency in the devices. To remedy this, the introduction of various ions into the perovskite crystal structure has been proposed. In order to determine how these substitutions affect films in controlled atmospheric conditions, *in situ* testing and a spectrum of material characterization measurements were completed. Namely, by altering the relative humidity in a sealed test chamber housing perovskite samples and subjecting the films to these controlled conditions over extended periods, degradation was observed. The effects of the addition of formamidinium (FA) and bromine ions into the perovskite crystal structure was tested through the fabrication of $MA_{0.7}FA_{0.3}PbI_3$ and $MA_{0.7}FA_{0.3}Pb(I_{0.9}Br_{0.1})_3$ films and comparing them to $MAPbI_3$ perovskite films. Characterizing the films yielded insight into the degradation pathway and kinetics. Overall, the addition of FA ions appeared to have adverse effects on the stability of the films while the addition of bromine ions appeared to increase the stability of the films from a humidity exposure standpoint. This was concluded as half-lives for the $MAPbI_3$, $MA_{0.7}FA_{0.3}PbI_3$, and $MA_{0.7}FA_{0.3}Pb(I_{0.9}Br_{0.1})_3$ films under 85% relative humidity were 31 hours, 9 hours, and 15 hours respectively. Using this data and experimentation method, a balance of device efficiency and film stability can be reached in order to find the best perovskite for general application.

Introduction

The demand for clean, renewable energy grows constantly as time progresses. As fossil fuels continue to be depleted, creating the alternative forms of energy has become paramount to offset the effects climate change and decrease of dependence on carbon dioxide emitting fuels. Harvesting solar energy has been identified as one of the key pieces to this puzzle. Recently, silicon based solar cells are becoming more affordable due to reduced manufacturing costs, allowing a broad spectrum of consumers from residential to commercial to purchase them. However, the price of these cells can only drop so far as essential energy intensive manufacturing processes and material cost cannot be avoided. In this way, new materials and manufacturing processes are necessary to continue the advancement of solar cell research.

Although silicon based, dye sensitized, and organic solar cells have been studied for over a decade, the research field of perovskite based solar cells has expanded rapidly (Hodes, 2013). The perovskite crystal structure was originally discovered in the 19th century, but it has only recently been used in solar cell devices. (Wang et al., 2016) The first paper detailing the use of perovskite materials in solar cell devices was published in 2009, even though the material dates back to a study completed by Weber (1978). (Jacobsson et al., 2016) With early power conversion efficiencies (PCEs) of 3.81%, perovskite solar cells have come a long way to their current 22.1% PCEs in a relatively short time. (Ali, et al., 2016) This spike in efficiency, along with their low cost and easy manufacturing processes, has made perovskite solar cells very popular among researchers today. A variety of manufacturing processes, such as sequential deposition, spin coating, and vacuum evaporation techniques have all yielded high efficiency perovskite devices. (Wang et al., 2016)

Perovskites act as a dye material in solar cells and are used to absorb sunlight. However, the absorption coefficient of perovskite films is estimated to be around 10 times higher than N719 dye, which is commonly used in dye sensitized solar cells (Ke et al., 2014) In a charge transport sense, perovskites are special in that they are capable of ambipolar diffusion, meaning that they can transport both electrons and holes when exposed to sunlight. The photons from sunlight penetrate the perovskite material and excite electrons within the solar cell. These excited electrons then jump the band gap between the valance and conduction bands within the perovskite, leaving a positively charged hole in the valence band. With other conductive materials surrounding the perovskite in the solar cell, these electrons and holes are transported out of the perovskite can collected separately so current and electricity can be generated (Gonzalez-Pedro et al., 2014).

Perovskites, named for their crystal structure, consist of an organic or inorganic cation, A, a metal cation, B, and a halide anion, X, in the form ABX_3 when used in solar cell applications (Ali, et al., 2016) This basic structure can be seen in Figure 1. Generally, perovskites used in solar cells consist of methylammonium (MA), lead, and iodine as $CH_3NH_3PbI_3$ or otherwise written as $MAPbI_3$. However, substitutions such as tin for the lead, formamidinium (FA) for the methylammonium, and chlorine or bromine for the iodine have all been explored as mixed halide and lead-free solar cell options. (Wang et al., 2016) With the intent of producing more stable and efficient films, detailed characterization techniques are often employed to fully understand the nature of the perovskites and their potential applications. This characterization generally includes structural, compositional, and electronic measurements.

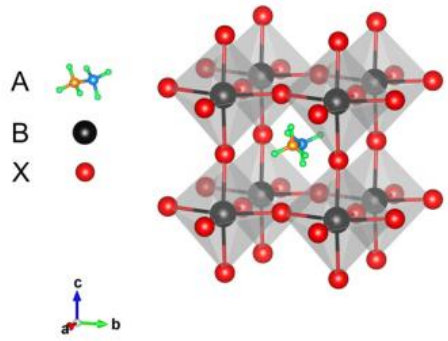

Figure 1: *Perovskite Crystal Structure (Wang et al., 2016)*

Perovskites have paved the way for efficient solar cell devices, but they are not without their short comings. Stability issues due to environmental factors have plagued perovskites and often lead to the deterioration of the perovskite layer, a loss of efficiency in the devices, and the potential for environmental exposure. Moisture in the atmosphere and exposure to high temperatures have been shown, through many studies, to inversely affect perovskite films. In order to fully understand how a perovskite will perform in varying environmental conditions, extensive testing must be completed with highly controlled conditions.

In order to fully examine the effects of humidity on perovskite materials, measurements over the degradation time must be taken. This allows researchers to see the nuances of the film degradation and the rate at which degradation occurs. *In situ* measurements in humidity controlled environment is the best way to accomplish this. Yang et al. (2015) pioneered this method, creating an experimental apparatus that allowed samples to be tested in controlled humidities, as seen in Figure 2b. The experimental setup used, as seen in Figure 2a, allowed for the strict control and regulation of the relative humidity (RH) in the system and insured a controlled experimental process. Through this measurement technique, features of the perovskite decomposition could be further examined. In addition, Yang et al. showed that the

experiment was repeatable and consistent when both nitrogen and air was used to complete the tests. In this way, either gas could be humidified and used for testing. (Yang et al., 2015)

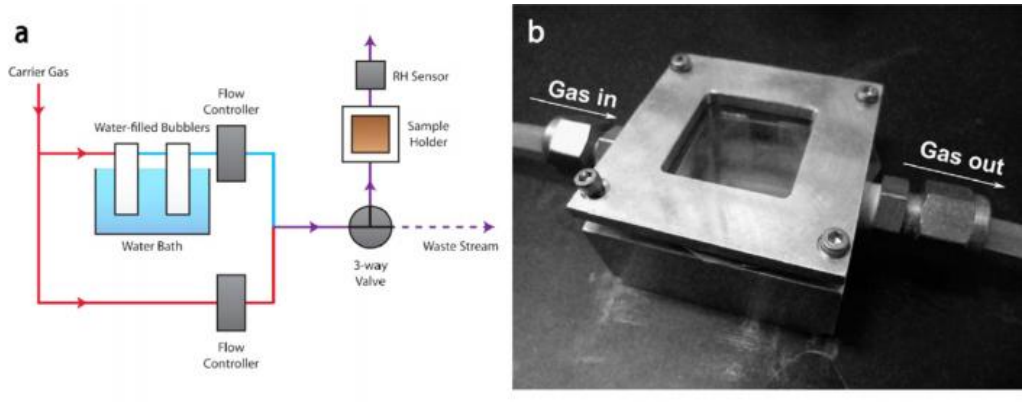

Figure 2: *(a) Experimental Setup (b) In situ testing device (Yang, et al., 2015)*

With this study, Yang et al. (2015) completed the ground work to allow for the testing and monitoring of perovskite degradation in controlled humidity environments. Using the techniques described in the study, further testing on perovskites with different compositions can be completed. By creating and testing perovskite films with varying ion substitutions, the effects of these substitutions with respect to humidity in the atmosphere can be explored.

Purpose

The purpose of these experiments was to determine how perovskite films with varying ion compositions react in controlled atmospheric conditions. Namely, by altering the relative humidity of a test chamber housing perovskite samples and subjecting the films to these controlled conditions over extended periods, degradation could be observed. Through this, critical points of degradation of the perovskite film could be identified through absorbance measurements. In addition, the half-lives of the films were determined. These measurements

were conducted in the test chamber by affixing the test film to the bottom and housing the chamber in the spectrophotometer. After determining degradation rates and times, the samples were assessed and characterized under various instruments. The assessment of cells included Fourier Transform Infrared Spectroscopy and Attenuated Total Reflectance (FTIR-ATR) measurements, X-Ray diffraction (XRD) measurements, and reviewing the surface via scanning electron microscope (SEM). In addition, three different perovskite recipies were tested. Different mixtures of lead iodide (PbI_2), lead bromide ($PbBr_2$), methylammonium iodide (MAI) and formamidinium iodide (FAI) were combined according to different studies to form varying perovskite films. In this way, the effects of substituting different ions into the perovskite crystal structure could better be understood by way of humidity induced degradation.

Background

Water Induced Degradation

Water in the form of atmospheric moisture has proven to be a key factor in perovskite degradation. In a study conducted by Tong et al. (2015), models were used to simulate the adsorption of water molecules onto $MAPbI_3$ perovskite structures. In the model, the water adsorbs to the surface of the perovskite crystal before diffusing into the structure itself. With a calculated diffusion barrier between the surface and inside region of the perovskite of 0.04 eV, water can penetrate the large interstitial space of the perovskite crystal structure. This water then interacts with the MA ion in the crystal structure, causing the corrosion of the structure through changing the orientation of the ion. A schematic of water ions infiltrating the perovskite crystal structure and its effects on optical absorption can be seen in Figure 3. (Tong et al., 2015)

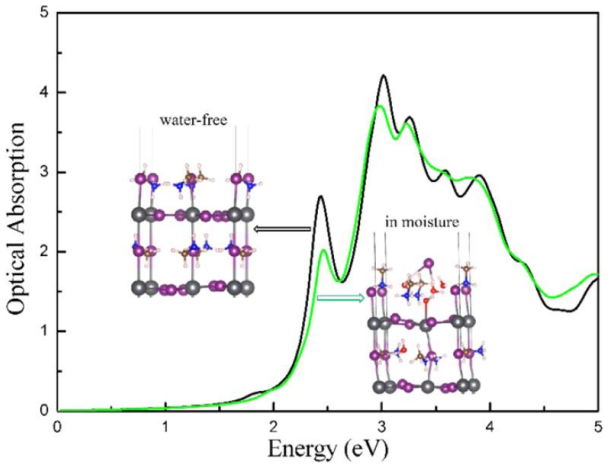

Figure 3: *The effects of water on perovskite crystals (Tong et al., 2015)*

This decomposition pathway of the perovskite can be seen in Figure 4a. With the addition of water, the perovskite structure is decomposed into methylammonium iodide and lead iodide. Further, the MAI is decomposed into hydriodic acid and methylamine resulting in a complete breakdown of the perovskite film. The chemical description of this decomposition is detailed in Figure 4b. The speed of this reaction is based on the amount of water that the films are subjected to.

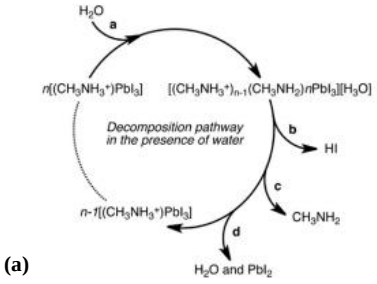

(a)

(b)

$$CH_3NH_3PbI_3 \overset{H_2O}{\Leftrightarrow} CH_3NH_3I(aq) + PbI_2(s)$$

$$CH_3NH_3I(aq) \Leftrightarrow CH_3NH_2(aq) + HI(aq)$$

$$4HI(aq) + O_2 \Leftrightarrow 2I_2(s) + 2H_2O$$

$$2HI(aq) \overset{h\nu}{\Leftrightarrow} H_2\uparrow + I_2(s)$$

Figure 4: *The decomposition pathway of $MAPbI_3$ perovskites due to water (Wang et al., 2016)*

In addition to the authors *in situ* absorbance testing, Yang et al. (2015) also performed *in situ* grazing incidence x-ray diffraction (GIXRD) measurements that showed the formation of a

hydrated compound, $(CH_3NH_3)_4\ PbI_6 \bullet 2H_20$ as a result of the humidity testing. This data suggests that a hydrated phase of the perovskite degradation exists as an intermediate in the decomposition of the films. This phenomenon was also observed by Christians et al. (2015) when the authors synthesized the dihydrate in the form a bright yellow precipitate. The XRD pattern for the dihydrate can be seen in Figure 5.

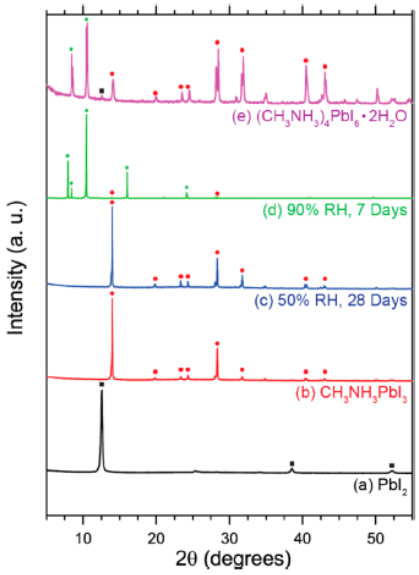

Figure 5: *XRD patterns of perovskites under various conditions (Christians et al., 2015)*

However, in another study completed by Leguy et al. (2015) XRD techniques were used to identify that a reversible monohydrate form, $CH_3NH_3PbI_3 \bullet H_20$ forms before the irreversible dihydrate form. The reaction pathway is detailed in Figure 6. The authors noted the formation of the monohydrate form after a perovskite film was exposed to 80% RH from 30 to 60 minutes. However, after 120 minutes in these conditions, dehydrate peaks were observed. In this way, Leguy et al. (2015) concluded that the perovskite hydration reaction is started when a single water molecule diffuses into the perovskite structure. This reaction is completely reversible.

With longer exposure to humid conditions, additional water molecules diffuse into the perovskite, causing the irreversible creation of the dihyrdated form, PbI_2, and water molecules. In this way, the degradation of a perovskite is catalyzed by the water molecules that can begin degrading or further degrade surrounding crystals. (Leguy et al., 2015)

$$4(CH_3NH_3)PbI_3 + 4H_2O \rightleftharpoons 4[CH_3NH_3PbI_3 \cdot H_2O]$$
$$\rightleftharpoons (CH_3NH_3)_4PbI_6 \cdot 2H_2O + 3PbI_2 + 2H_2O$$
$$(CH_3NH_3)_4PbI_6 \cdot 2H_2O(s) \xrightarrow{H_2O(l)} 4CH_3NH_3I(aq) + PbI_2(s) + 2H_2O(l)$$

Figure 6: *Formation pathway for monohydrate and dehydrate perovskites (Leguy et al., 2015)*

Substitution Ion Selection

The idea behind ion substitution is to create a better performing perovskite film. In many cases, this is done to create a more efficient solar cell device or to tune the band gap of the perovskite layer for use as in a tandem solar cell. Jacobsson et al. (2016) noted that for perovskite cells to compete with silicon based cells, a more efficient and less expensive cell would have to be fabricated. Although advances leading to increased perovskite cell efficiencies have been found, the authors argue that use in a tandem cell may be the best application of the technology. Instead of producing highly efficient and expensive silicon cells, combining a moderately efficient silicon cell with a perovskite cell with an ion tuned band gap could generate higher efficiencies at a lower cost. This can be seen in Figure 7. Since perovskite cells are best used as top cells in tandem cells and silicon has a band gap of 1.1 eV, tuning the band gap of the perovskite to 1.72 eV could produce highly efficient solar cells. This would alleviate the cost

associated with manufacturing the best possible silicon cell by incorporating a less expensive perovskite cell to boost the overall efficiency. (Jacobsson et al., 2016)

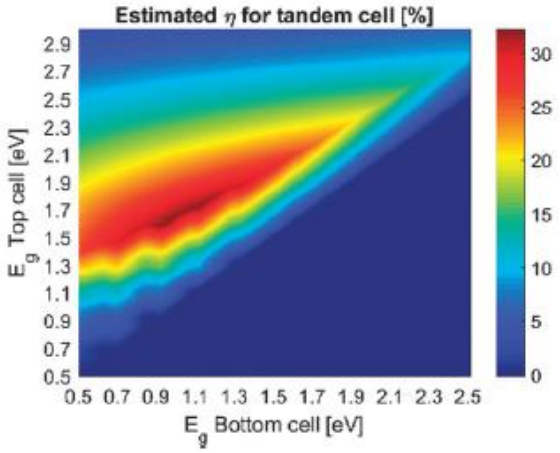

Figure 7: *Estimated efficiencies of tandem solar cells based on the band gap of the top and bottom cells. (Jacobsson et al., 2016)*

At the current time, most of the research focus is on creating the next record solar cell device, and less on enhancing the stability of the films in regard to atmospheric moisture. Formamidinium and bromine ions have recently been shown to offer positive enhancements to perovskite performance through increased crystallinity and band gap tuning.

With the addition of FA ions to the $MAPbI_3$ perovskite, the study by Yang et al. (2016) showed an absorbance shift from 790 nm to 840 nm as the percent FA in the film increased from 0% to 100%. Similarly, the band gap energy decreased from 1.61 eV to 1.51 eV and the XRD peak shifted from 14.22° to 13.95° for $MAPbI_3$ and $FAPbI_3$ respectively. This represents a conversion of the tetragonal phase $MAPbI_3$ perovskite to a trigonal phase $FAPbI_3$ perovskite. This conversion can be seen in Figure 8 and indicates that the FA ions were homogeneously incorporated into the $MAPbI_3$ crystal structure. Through testing to determine the best hybrid

perovskite based on power conversion efficiency (PCE), a $MA_{0.7}FA_{0.3}PbI_3$ perovskite was identified. (Yang et al., 2016) The PCE is determined using open circuit voltage (V_{OC}), fill factor (FF), and short circuit current (I_{SC}) of the solar cell along with the power of the incident sunlight (P_{in}) using the equation $PCE = \frac{I_{SC}V_{OC}FF}{P_{in}}$.

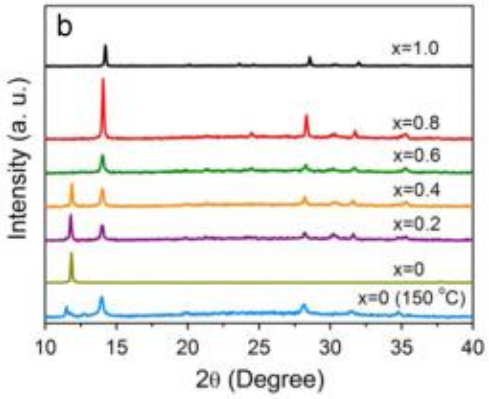

Figure 8: *XRD spectrum of $MA_xFA_{1-x}PbI_3$ (Yang et al., 2016)*

Pallet et al. (2014) also found that using a majority of MA ions in $MA_{0.6}FA_{0.4}PbI_3$ generated efficient solar cells, remarking about the decreased presence of the δ-phase FA perovskite formed with increased MA content. (Pallet et al., 2014) This non-perovskite, yellow colored δ-phase if formed more easily than the black α-phase perovskite due to is lower formation energy, causing pure $FAPbI_3$ films to be difficult to fabricate. (Yang et al., 2016) With an optimized MA:FA ratio, the effects of bromine ions could be determined.

Similarly to the FA ions, Br^- ions were also homogeneously incorporated into the $MA_{0.7}FA_{0.3}PbI_3$ crystal structure. When the bromine ion content increased from 0% to 20%, Yang et al. (2016) showed an absorbance shift from 800 nm to 750 nm and a change in band gap energy from 1.57 eV to 1.69 eV was observed. In addition, the incorporation of Br^- ions shifted the XRD peak from 14.10° to 14.30°, showing a gradual change from a tetragonal phase to a

more stable cubic phase. This shift can be seen in Figure 9. This improved crystallinity also increases carrier lifetime and decreases the density of trap states in the films and consequently increases PCE. Similarly to the FA trials, testing was completed to determine the best perovskite composition and a $MA_{0.7}FA_{0.3}Pb(I_{0.9}Br_{0.1})_3$ perovskite was identified. (Yang et al., 2016) Berdiyorov et al. (2015) also found that the addition of small amounts of Br^- ions significantly increased the electron transport of $MAPbI_3$ perovskites due to higher crystallinity, corresponding to an increase in solar cell efficiencies. (Berdiyorov et al, 2015)

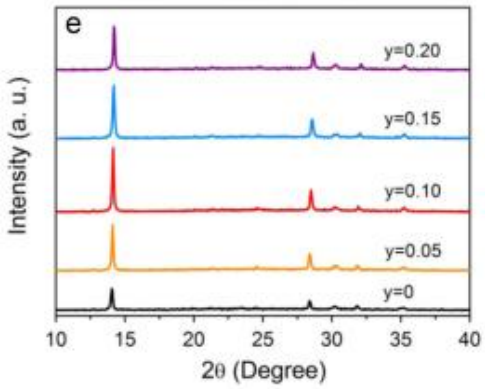

Figure 9: *XRD spectrum of $MA_{0.7}FA_{0.3}Pb(I_{1-y}Br_y)_3$ (Yang et al., 2016)*

Wang et al. also described an experiment that captured the effects of increased Br ion content on perovskite film stability. Four perovskite solar cells were created with varying Br content, as seen in Figure 10. The initial efficiencies of these cells were measured and the cells with lower Br ion content were more efficient, as would be expected. After this initial test, the films were subjected to a 35% RH environment for 3 days and minor changes in the cell efficiencies were observed. However, the cells were then subjected to 55% RH on the fourth day and the cells with little to no Br content experienced large drops in efficiency. Conversely, the

cells with increased Br content remained unchanged even with the increased RH. Beyond this, the cells with high iodine content continued to degrade under the 35% RH atmosphere while the other cells kept their efficiency. (Wang et al., 2016)

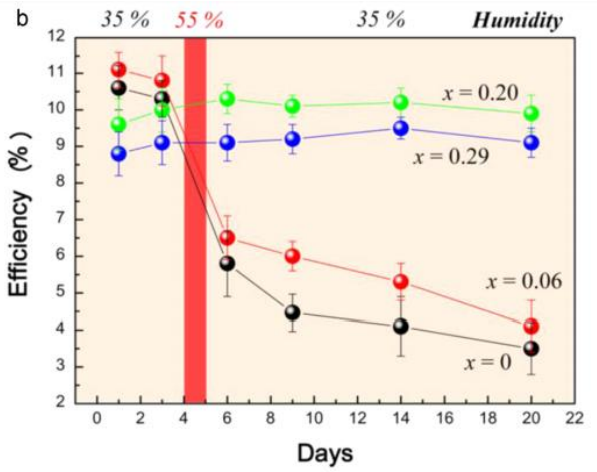

Figure 10: *The effects of prolonged humidity exposure on $MAPb(I_{1-x}Br_x)_3$ (Wang et al., 2016)*

In another study by Reuss et al. (2016), perovskite films with varying fractions of bromide and iodine ions were subjected to 67±5% RH atmospheres and observed, as seen in Figure 11a. It can be seen to the naked eye that the higher iodine content films were influenced far more greatly than the higher bromine content films. This effect can also be seen in Figure 11b as the absorption spectra show little degradation in the bromide rich films over time. The authors found that by increasing the bromine content of the films, the perovskites became less susceptible to the moisture in the air by suppressing the transformation of the perovskite into a hydrated phase. The monohydrate form, $CH_3NH_3Pb(I_{1-x}Br_x)_3 \cdot H_2O$, was observed in sample with high iodine contents and samples with high bromine contents tended to not transform. This was thought to be due to the strong hydrogen bonding observed between the bromine and MA ions. (Reuss et al., 2016)

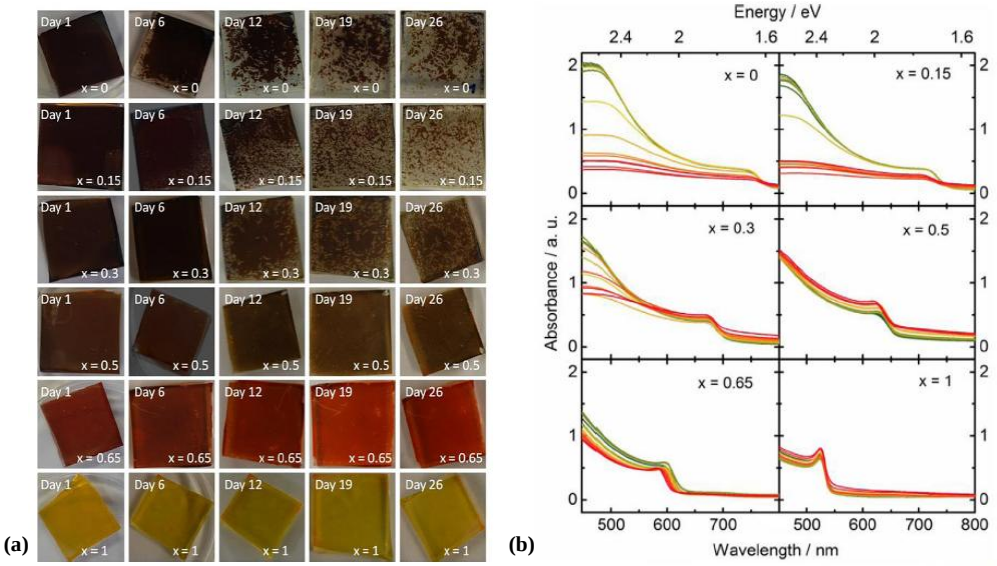

Figure 11: *$MAPb(I_{1-x}Br_x)_3$ degradation images (a) and associated absorption spectra (b) (Reuss et al., 2016)*

Further testing concluded that the incorporation of FA and Br^- ions decrease the activation energy for boundary mobility, leading to larger grain sizes and improved crystallinity in the perovskite films. In addition, the addition of these ions decreases the number of defects in the perovskite films, increasing the potential performance for solar cell usage. Beyond this, both ions can be used to tune the band gap of the perovskite film being created. (Yang et al., 2014)

In addition to band gap tuning, many studies have shown that FA and Br^- ions can be used to tune the optical color of perovskite films, ranging from dark brown to yellow or red. In a study completed by Cui et al. (2015), the Br content in $MAPbI_3$ perovskites was systematically altered in order to color-tune the films for potential use in building applications. Figure 12 depicts the results of the study. Through simple changes in ion substitution, the films ranged from a yellow $MAPbBr_3$, to a red $MAPbBr_2I$, and to the well documented dark brown $MAPbI_3$.

The corresponding efficiencies for these films ranged from 3.53% to 12.76% for the $MAPbBr_3$ and the $MAPbI_3$ respectively. In this way, it was shown that color tuning perovskite films for specific applications beyond highly efficient solar cell use is possible using Br^- ions. (Cui et al., 2015)

Figure 12: *Color Tuning perovskites with varying I:Br ratios (Cui et al., 2015)*

Recently, a study completed by Jacobsson et al. (2016) explored the effects of changing both the MA:FA and Br:I ratios on color tuning perovskite films. Their matrix of samples can be seen in Figure 13.

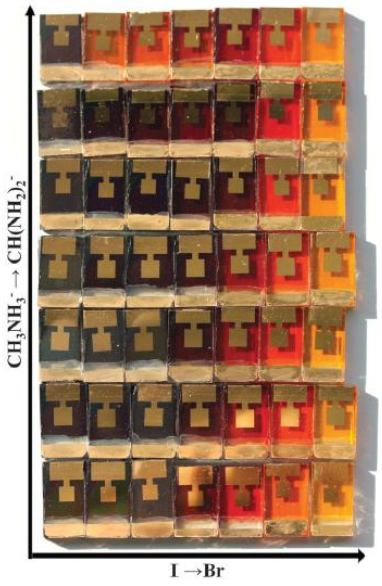

Figure 13: *Color Tuning perovskites with varying I:Br and MA:FA ratios (Jacobsson et al., 2016)*

The perovskite films with larger portions of iodine tended to be a dark brown color compared to the red and yellow color present with larger portions of bromine. This is consistent with the Cui et al (2015) study. In the case of substituting FA for MA, there is not a large difference in the color until the film is $FAPbBr_3$. The authors noted that this is likely due to the yellow hexagonal FA polymorph. When viewing the films under SEM, the iodine containing films were smooth with limited number of pinholes. The films containing a majority of bromine appeared smoother, but also cracked under the SEMs electron beam, potentially indicating more fragile grain boundaries. In addition, the authors also confirmed that Br increases the band gap, while FA decreases it. Interestingly, the authors also noted that XRD data often showed an excess of PbI_2 in the mixed perovskites. In this way, they believe that $PbBr_2$ forms perovskites more readily than PbI_2. This is an interesting observation as iodine based perovskites produce more efficient solar cells, as seen in Figure 14, but bromine based perovskites crystallize more readily. (Jacobsson et al., 2016)

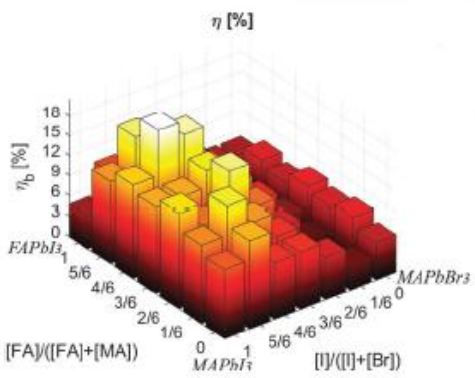

Figure 14: *Efficiencies of perovskites with varying I:Br and MA:FA ratios (Jacobsson et al., 2016)*

Temperature Induced Degradation

Temperature also plays a large role in the life of a solar cell. Even before it is subjected to the intense heat to the sun for many hours a day, perovskite layers must be annealed onto the surface of the cell. Many studies found that increased temperature and duration of heating causes the perovskite film to break down into lead iodide prematurely. In one study by Supasai et al. (2013), GIXRD was used to verify that after heating a $MAPbI_3$ to 100°C for 30 minutes, no lead iodide diffraction peaks were present. It was also noted that annealing the films at 140°C and 160°C induced decomposition to PbI_2. These conclusions can be seen in the spectra in Figure 15. (Supasai et al., 2013)

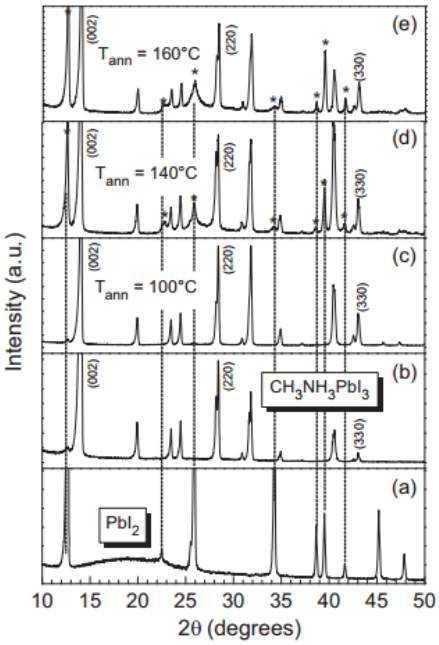

Figure 15: *GIXRD spectra of perovskite film annealed at different temperatures (Supasai et al., 2013)*

However, a study completed by Bag et al. (2015) showed that the addition of FA ions into the $MAPbI_3$ crystal lattice helps provide photostability through lowering the absorption of

infrared light. The authors noted that perovskite photodegradation occurs over the infrared due to increased ion transport in the $MAPbI_3$ films. The addition of FA ions alters the absorption characteristics of the films by increasing the energy necessary for ion diffusion, providing improved stability. (Bag et al., 2015) In addition, the addition of FA showed an increased temperature stability as FAI perovskites remain stable up to 150°C, while the presence of the MA ions allow them to be formed at 100°C. (Wang et al., 2016)

Methods

The experimental set up consisted of humidifying a stream of nitrogen to a given relative humidity before sending it into the test chamber (Figure 16). The test chamber was 256 cm^3 and was made of borosilicate glass adhered with glass glue and sealed with silicone caulk. The removable lid sealed to the base through a silicone gasket that could be fastened using tape so no leaking would occur. The outlet of the chamber was an eighth inch tube to prevent back diffusion from the lab atmosphere. The input to the chamber was a single quarter inch tube that combined the flow from two separate lines.

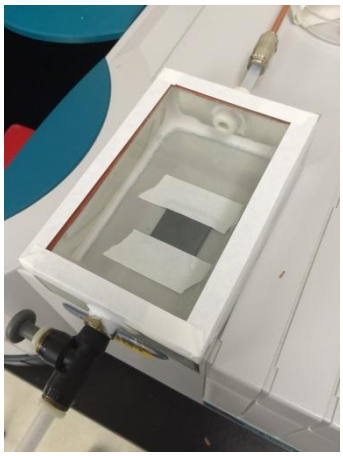

Figure 16: *Humidity Test Chamber*

The nitrogen flow from a bottle was divided between a straight line to the chamber and a line that passed through a deionized water bubbler to create saturated gas. Using a hygrometer, the relative humidity measurements were verified before each test via in situ readings. Upon testing, the bubbler was found to produce a maximum of 85% relative humidity. The flow in these "wet" and "dry" lines was controlled by volumetric flow meters that could be manually set to alter the humidity level in the chamber. In the case of the 30% relative humidity test, the dry line was set to 0.088 L/min and the wet line was set to 0.162 L/min. In this way, the 0.25 L/min total flowrate consisted of 30% moist gas, giving the correct relative humidity for the test. Similarly, in the case of the 50% relative humidity test, the dry line was set to 0.103 LPM and the wet line was set to 0.147 L/min. Finally, in the case of the 80% relative humidity test, the dry line was set to 0 L/min and the wet line was set to 0.25 L/min. A schematic of the experimental set up is detailed in Figure 17 and a picture of the actual set-up is provided in Figure 18.

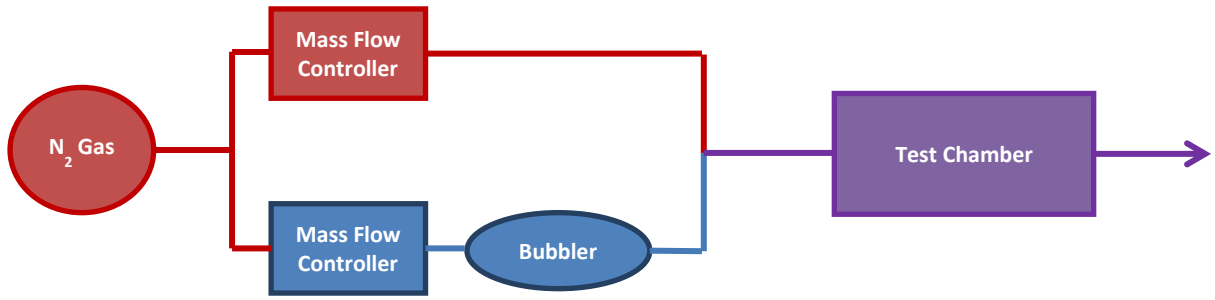

Figure 17: *Experimental Set-up Schematic*

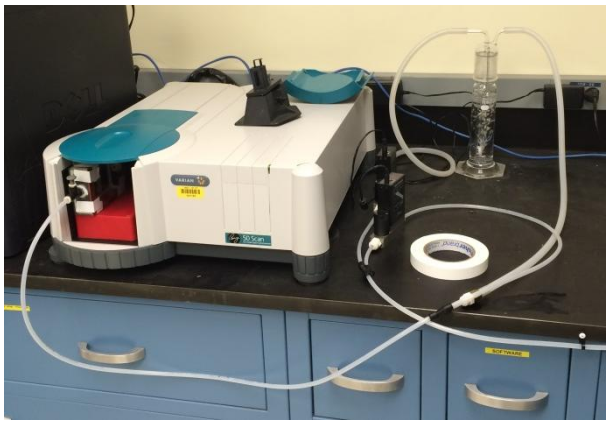

Figure 18: *Experimental Set-up*

Gloves and Safety glasses were worn at all times to avoid cuts, burns, and chemical exposure. All samples were made on fluorine doped tin oxide (FTO) glass or borosilicate microscope slides. The glass selection depended on the instrument the sample was being tested in. All glass was cut using a glass cutter to score glass and the pieces were broken using "glass scissors". Glass pieces were then thoroughly cleaned and dried. Water with RBS detergent was added to container so that glass was completely covered and the container was sonicated for 5 minutes. The container was then emptied and the glass was rinsed in the container with DI water. Additional DI water was poured into container so that glass is completely covered and the glass was sonicated again for 5 minutes. The container was emptied of water and ethanol was added until the glass pieces were completely covered. The container was then sonicated for 5 minutes before emptying the ethanol into an appropriate Hazardous Waste container. The glass pieces were then dried in an oven at 70°C for an hour.

The perovskite recipes used were adapted from reports by Correa Baena et al. (2015) as well as Yang et al. (2016). For the first perovskite, a solution of 1.2 M lead iodide (1.3830 g) and 1.2 M methylammonium iodide (MAI) (0.4769 g) in 0.5 ml of dimethylsulfoxide (DMSO)

and 2 ml dimethylformamide (DMF). This recipe is commonly used in studies and is a good baseline for additional testing. To test the effects of substituting anions and cations, lead bromide and formamidinium iodide (FAI) were added to the perovskite solutions. The second perovskite tested was a solution of 1.2 M lead iodide (1.3830 g), 0.36M FAI (0.1548 g), and 0.84 M MAI (0.3338 g) in 0.5 ml of DMSO and 2 ml DMF to form $MA_{0.7}FA_{0.3}PbI_3$. The third and final perovskite was a solution of 1.02 M lead iodide (1.1756 g), 0.18 M lead bromide (0.1652 g), 0.36 M FAI (0.1548 g), and 0.84 M MAI (0.3338 g) in 0.5 ml of DMSO and 2 ml DMF to form $MA_{0.7}FA_{0.3}Pb(I_{0.9}Br_{0.1})_3$. In all cases described, the perovskites were formed by adding the solid materials to a vial before adding the liquid materials. A quarter inch stir bar was added to each vial and the solutions were stirred for 24 hours to ensure they were homogeneous. Before using the solution, each was subjected to a 0.22 μm filter.

When preparing the perovskite films, clean, room temperature glass pieces were placed into a spin coater and secured using the suction from a vacuum pump. 150 μl of perovskite solution was then pipetted onto the middle of the surface of the glass. The sample was then subjected to 1000 RPM for 10 seconds followed by 4000 RPM for 20 seconds. 10 seconds before the second 4000 RPM step was finished, 100 μl of chlorobenzene was applied rapidly to the middle of the spinning film through a pipette held perpendicular to the glass. The glass pieces were then removed from the spin coater and placed onto a hot plate in an environment with a relative humidity under 20% for 30 minutes. The samples were then cooled and stored in a desiccator until testing occured. Fresh samples were made for each test completed.

To test the films, the borosilicate glass piece with the perovskite film was affixed to the base of the chamber before it was sealed. The chamber was then mounted onto the side of the UV-vis spectrophotometer so that the machine's beam passed through the lid, sample, and

bottom of the chamber when scanning. A background scan of the ambient air and test chamber were taken before testing began. Samples were scanned at defined intervals for 24 hour periods. In this way, the half-life of the films could be found. With this data, experimental times were concluded for future tests.

Secondary tests were performed in a similar way to the absorbance testing. Perovskite films were subjected to 30% and 50% relative humidity for 48 hour periods. The samples were then removed from the chamber XRD and FTIR-ATR measurements were taken to help characterize the films. When using the XRD, samples were scanned from 5 to 55° at a scan rate of 2° per minute.

In conjunction with the humidity testing, initial testing on the fabrication and testing of solar cells was completed, as discussed previously. Cells were assembled stepwise, with each layer consisting of different chemicals and annealing methods. On a basic level, cells consisted of a titanium dioxide electron blocking layer, a titanium dioxide mesostructured layer, a perovskite layer, a hole transport layer, and silver electrical contacts. After construction, the cells were kept in a humidity free environment until the time of testing. After testing is completed, waste cells will be disposed of properly as hazardous waste. A general schematic of the solar cell can be seen in Figure 19.

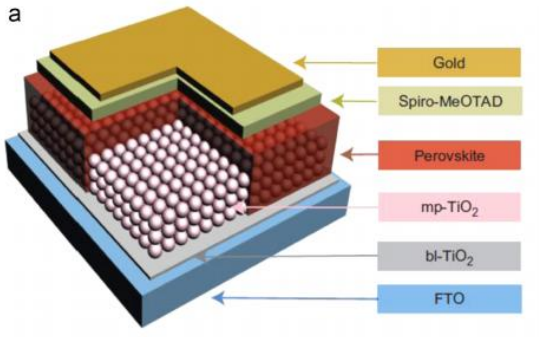

Figure 19: *Perovskite solar cell schematic (Wang et al., 2016)*

After the FTO glass was cleaned the titanium dioxide blocking layer was applied via the spin coater. 50µl of blocking layer solution was pipetted onto the glass and spun at 2000 RPM for 60 sec. After this, the glass was removed from the spin coater, placed on a titanium hot plate, and sintered at 500°C for 2 hours. Second, the titanium dioxide mesoporous layer was applied via the spin coater. 100µl of mesoporous layer solution was pipetted onto the glass and spun at 2000 RPM for 60 sec. The glass was then removed from spin coater, placed on a titanium hot plate, and sintered at 500°C for 2 hours. Next, the desired perovskite layer was applied via the spin coater. After the perovskite layer, the spiro hole transport layer was applied via the spin coater. 100µl of sipro solution was pipetted onto the glass and spun at 2000 RPM for 60 sec. The glass was then removed and stored without heating. Finally, silver contacts were applied to the cells via thermal deposition through a shadow mask. Contacts were 200 nm thick.

The blocking layer is a mixture of 369µl of titanium iospropoxide, 35µl of HCl, and 5.06 ml of isopropanol. The solution was prepared by measuring 2.53 ml of isopropanol into seperate vials. Titanium iospropoxide was added to one vial and HCl was added to the other. A 0.25" stir bar was them placed in each vial and allowed to stir for 30 seconds. After this time, the HCl solution was added to the titanium iospropoxide solution dropwise while stirring continued. Finally, before use, the solution was subjected to a 0.2 µm filter.

The titanium dioxide mesoporous layer was composed of a 6:1 ratio of terpinol and TiO_2 paste. To make the solution, an amount of TiO_2 paste was measured into a vial. The mass off this paste was found and, using the density of terpinol, a volume of terpinol equal to 6 times the mass of the paste was added to the vial. A 0.25" stir bar was then placed into the vial and stirred until the paste had dissolved completely.

The hole transport layer is a mixture of 2 ml of chlorobenzene, 23.44 ml TBP, 0.01435 g bis(trifluoromethane)sulfonamide lithium salt (LiB), and 0.14g spiro. All of the solids were added to a vial before the chlorobenzene and 4-tert-butylpyridine (TBP) were added. A 0.25" stir bar was placed in the vial and the solution was stirred until the solids dissolved completely.

Initial Background Testing

Testing began by creating $MAPbI_3$ perovskite films for testing in solar cells based on previous literature recipes. The initial perovskite tested was a $MAPbI_2Cl$ mixed halide perovskite based off of the recipe found in the study completed by Docampo et al. (2013). In these perovskites, 0.85485 g of $PbCl_2$ and 1.4667 g of MAI were combined in 2.5 ml DMF to form a 1.2 M solution. The solution was then spin coated onto glass at 2000 RPM and heated to 100°C for 45 minutes. However, after creating solar cells with the perovskite film, low efficiencies were discovered. In an attempt to characterize each layer to find the problem, each was reviewed under the SEM. The FTO layer was pristine as it was previously prepared on the glass before it was purchased. The titanium dioxide blocking layer, found in the Docampo et al. (2013) study, appeared as a very dense and thin film. Blocking layers are meant to deter carrier recombination at the FTO and perovskite interface and avoid the short circuiting of the solar cell. (Gao et al., 2015) However, small holes appeared in the film, as seen in Figure 20, raising further questions on its effectiveness.

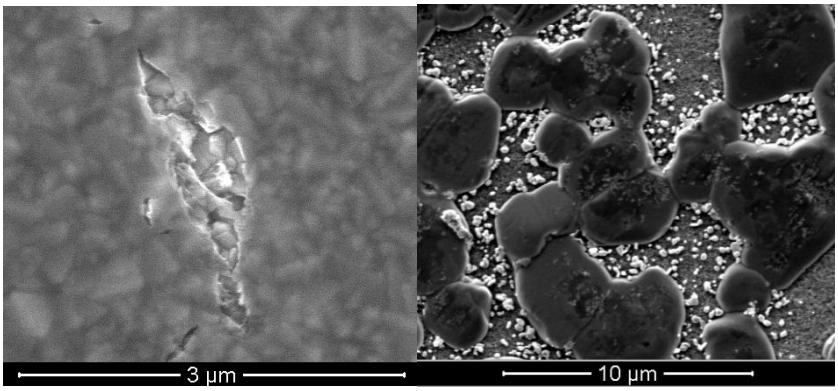

Figure 20: *Titanium Dioxide Blocking Layer (left) and $MAPbCl_3$ Perovskite (right) under the SEM*

Further testing was completed to compare the current through a plain FTO film and one with the blocking layer masking it. The data presented in Figure 21 was found through a cyclic voltammetry (CV) scan using a piece of FTO glass and a piece of FTO glass with the blocking layer sintered onto it as the working electrodes for each respective test. In the tests, a 0.1 M solution of tetrabutylammonium hexafluorophosphate ($TBAPF_6$) in dichloromethane (DCM) was used for the supporting electrolyte, a platinum wire rinsed with DCM was used as the counter electrode, and the reference electrode was Ag/Ag^+ as a 0.01 M solution of $AgNO_3$ in the supporting electrolyte. It can be determined based on the results of the scan that the blocking layer inhibits the flow of electrons, providing a smaller current compared to the plain FTO sample over the voltage sweep from -1.5 V to 1.5 V.

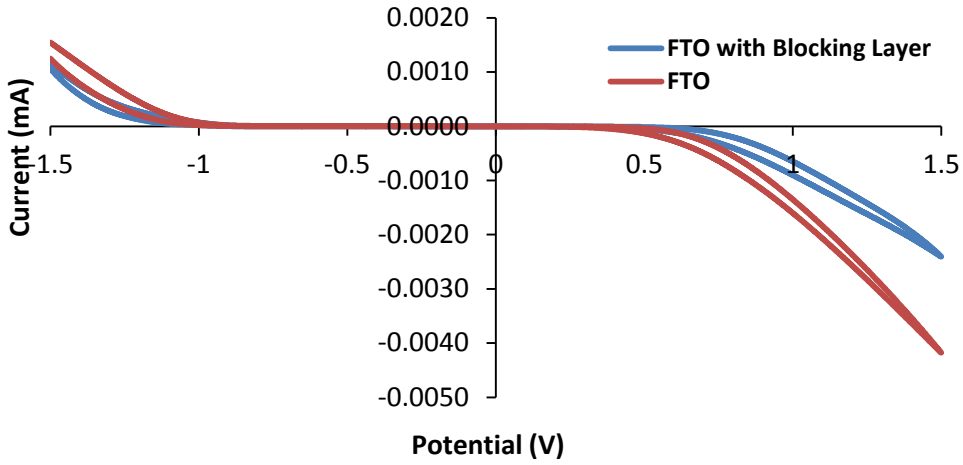

Figure 21: *CV Scan testing the effectiveness of the titanium dioxide blocking layer.*

Attention was the moved to the perovskite layer. Looking at the film with the naked eye, the film appeared grey and cloudy. Through inspection under the SEM, the films looked porous and created an incomplete layer, as seen in Figure 17. Similar images were discovered in a study completed by Wozny et al. (2015), showing the effects of RH on films while they are being made. Figure 22 depicts the effects of increased humidity on the formation of perovskite films.

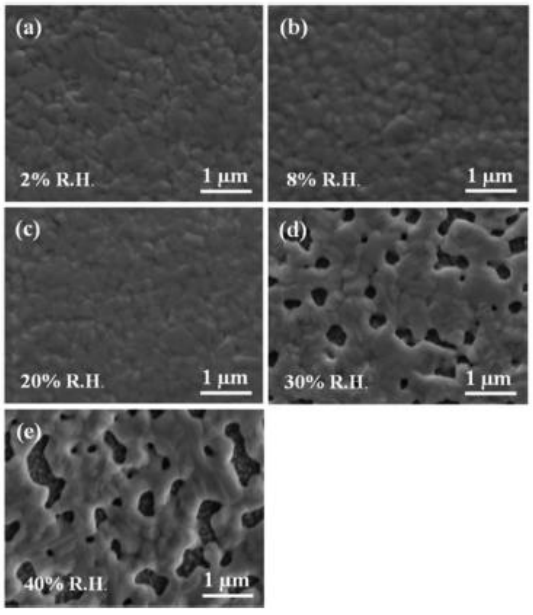

Figure 22: *The effects of humidity on perovskite film formation (Wozny et al, 2015)*

With this information, it became clear that relatively high amounts of moisture in the air had a direct and detrimental effect on the formation of pristine films. It was also noted that films created below 20% RH showed little effect from the moisture in the air. (Wozny et al, 2015) As the SEM picture in Figure 19e was similar to the perovskite in Figure 17, it became apparent that the effects of humidity on perovskite films should be investigated further.

With additional research, information showed that most recipes had begun to shift away from using chloride, and toward using iodide instead. This substitution was favored due to the increased absorbance of the perovskite films when iodide was used, leading to increased solar cell performance. In addition, studies such as Correa Baena et al. (2015) also showed that the introduction of toluene or chlorobenzene provided enhanced crystallization of the perovskite film, further enhancing the absorption properties.

Initially, the methylammonium iodide used to create the perovskites was created in the lab from precursor solutions. However, purity concerns surfaced when the perovskites formed as streaky films instead of uniform surfaces. These "star" patterns, as seen in Figure 23a, were deemed to be caused by the use of impure substances.

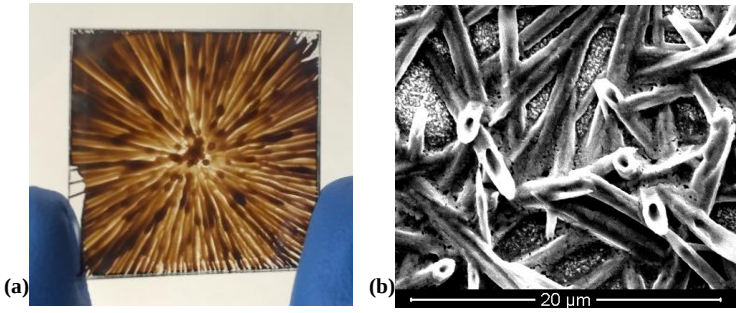

Figure 20: *(a)"Star" pattern and (b) nano tubes formed as an imperfect perovskite layer*

To remedy this, pure materials were purchased from Dyesol. In addition, by honing in on the drop casting technique through specific timing of the chlorobenzene application, uniform films were produced. In addition to the "star" patterns, special care had to be taken to avoid prematurely drying the films. By applying the chlorobenzene too early, cloudy, off color films were produced. When checked under the SEM, perovskite nanotubes were found instead of a uniform crystalline film, as seen in Figure 23b. Through extensive testing and refining the fabrication process, pristine films were eventually formed.

Attention was then switched to humidity testing the perovskite layers, as the humidity in the air had a marked impact on the surface morphology of the films. Specifically, after prolonged exposure to the atmosphere, the dark films turned yellow as the perovskite films degraded. The reasoning behind this was to increase the lifetime of the perovskite films and find alterations to the perovskite that would enhance stability in moist environments. In order to quantify this, tests were run to test the effects of low (30%) and high (95%) humidity over short periods of 3 hours.

The data collected showed promising results. The FTIR-ATR data shown in Figure 24 indicated large decreases in features that were attributed to N-H and C-H stretches in a study by Jeon et al. (2014) with increased humidity exposure, suggesting loss or hydration of methylammonium. In addition, the absorbance spectrum shown in Figure 24 indicated that high humidity leads to faster degradation of the films. As seen in previous studies, exposure to low humidity for a short time produced a small difference in the absorbance of the films.

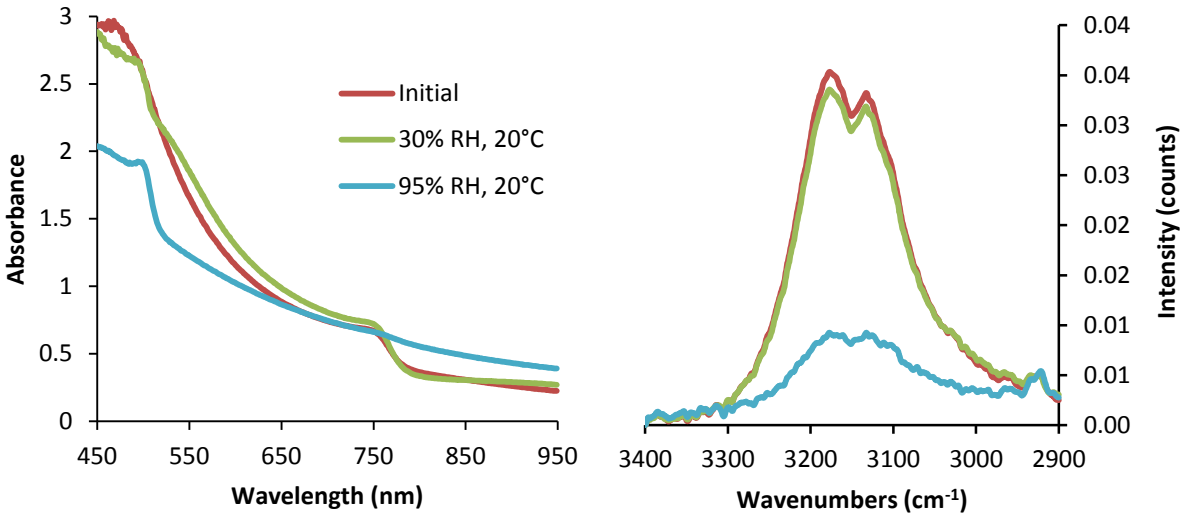

Figure 24: *Absorbance spectrum (left) and FTIR data (right) for $MAPbI_3$ perovskite films after 3 hours of exposure*

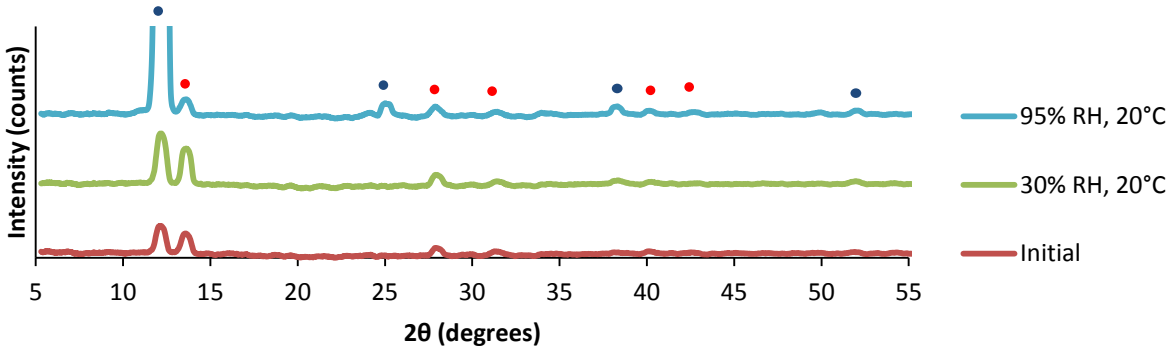

Figure 25: *XRD Spectra for $MAPbI_3$ perovskite films. Perovskite and lead iodide peaks are labeled using red and blue dots respectively.*

Finally, the XRD plot shown in Figure 25 showed the conversion of CH_3NH_3I to PbI_2 with increased humidity. In Figure 25, the peaks under the blue dots indicate the crystal structure of PbI_2 while the red dots indicate the $MAPbI_3$ peaks. The peaks associated with PbI_2 grew strongly after the exposure to high humidity, but were not noticeable when exposed to the low humidity. Although the initial sample appeared to contain PbI_2, transportation to the XRD

machine under humid conditions was cited for this premature degradation. In addition, even under high relative humidity, the perovskite crystal peaks remained. In this way, even thought they were diminished, the perovskite film was not completely degraded.

With this data, it was determined that additional testing would reveal degradation rates and properties of the perovskite films. Specifically, measuring the absorbance of films over time and tracking the film degradation would provide insight on the stability of perovskites and the applicability in the field.

Solar Cell Testing

When testing solar cells, electrodes were connected to a current/voltage (I/V) sweeping machine to find the I/V curve and test efficiencies. However, the cells were initially connected with alligator clips and masked with electrical tape. These connections lead to poor electrical connections and puncturing of the evaporated electrodes on the cells. This lead to inaccurate I/V measurements and poor results. To remedy this, a solar cell testing device was developed and manufactured. Instead of attaching the alligator clips directly to the cell, they were clipped onto wires that were soldered into springs to create non-destructive electrical contacts. These springs were spaced to make contact with the end of each test strip and with the ground strip on the cells in a plastic housing with a guide to seat the cells correctly. Finally, a cover was created with a slit cut through the middle at a width of 4 mm. In this way, the test area of each cell was confined to exactly 0.12 cm^2 for each trial. Using the holder increased the accuracy of the trials and allowed cells to be reused more frequently. Pictures of the solar cell holder can be seen in Figure 26. In addition, I/V curves found using alligator clips and the holder can be seen in Figure 27.

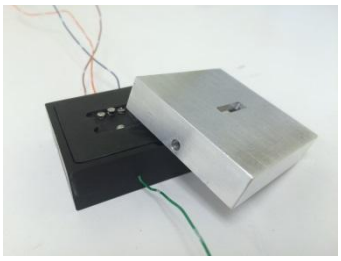

Figure 26: *Solar Cell Testing Device*

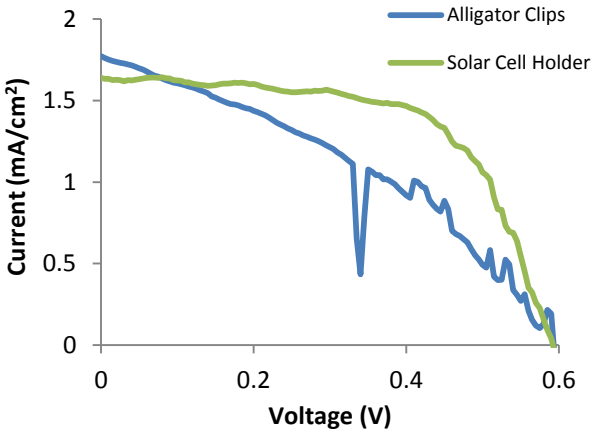

Figure 27: *Solar Cell Testing Comparison*

In addition to illustrating the merits of the solar cell testing device, Figure 27 also illustrates results from the testing of solar cell devices. Initial testing of the $MAPbI_2Cl$ solar cell devices produced a maximum efficiency of 2.77%. In an attempt to improve this efficiency of future devices, $MAPbI_3$ was utilized as the new perovskite layer in the cell. The best efficiency reading found during the testing of the $MAPbI_3$ cells, 5.02%, was garnered from the green I/V curve in Figure 27. Although this was an increase in efficiency, neither of these reading were close to the reported values in published literature. There are numerous potential causes of degradation of perovskite-based solar cell devices, which will be briefly summarized.

Beyond environmental conditions that lead to perovskite degradation, integration into solar cells provides its own problems for the films. In most solar cells, a hole transport layer is applied directly on top of the perovskite layer to ensure efficient hole transport out of the material. As discussed by Wang et al. (2015), the most commonly used hole transport material is Spiro-OMeTAD, which requires additives to improve conductivity. However, the 4-tert-butylpyridine and bis(trifluoromethane)sulfonamide lithium salt used also degrades the perovskite film. In addition to the hole transport layer, the evaporated metal contacts used as electrodes on the solar cell can also have an effect on the perovskite layer. Although gold is used as an electrode in high efficiency solar cells, silver is also used to minimize cost. However, studies have shown that silver is more environmentally unstable. When exposed to moisture in the atmosphere, pinholes can form in the spiro layer, allowing the moist air to interact with the perovskite layer. With this, the perovskite degrades and iodine containing species migrate through the spiro and diffuse into the silver contact, creating AgI. (Wang et al., 2016)

Due to the complexity of the solar cell devices and the many factors that can impair their performance, the remainder of this study focused on testing and characterization of the perovskite layer itself.

Results and Discussion

To further the research on *in situ* monitoring of perovskite degradation, perovskites utilizing FA and Br ions were tested. These perovskites were chosen based on commonly used recipes found in literature and utilizing ion substitutions that have known benefits to perovskite efficiency and stability. The following are measurements characterizing the perovskites used in the experimentation. In the trials, the films were tested until they reached their "end of life"

(EOL) under an 85% RH to ensure a full degradation spectrum was collected. The EOL was determined based on literature values and the change in absorbance of the films over time. When the absorbance readings plateaued, the trial was stopped. Using this data, the half-life of each film was found by calculating the time it took to reach the midpoint between the initial and final absorbance values at 410 nm. After, the effects of 30% RH and 50% RH were explored by exposing the films for 2 days to these conditions. In addition, initial measurements of each film were taken as a base line.

Initial absorbance readings of the three perovskite films were taken and can be seen in Figure 28. Using the well documented absorbance spectra of $MAPbI_3$ as a baseline, the $MA_{0.7}FA_{0.3}PbI_3$ and $MA_{0.7}FA_{0.3}Pb(I_{0.9}Br_{0.1})_3$ perovskite films were compared and characterized. Although both $MAPbI_3$ and $MA_{0.7}FA_{0.3}PbI_3$ both show an increase in absorbance around 760 nm, the effects of the inclusion of FA into the perovskite crystal structure can be seen as both the $MA_{0.7}FA_{0.3}PbI_3$ and $MA_{0.7}FA_{0.3}Pb(I_{0.9}Br_{0.1})_3$ perovskite films exhibit similar absorbance spectra below 700 nm. As the common factor in both of these films is the addition of FA, this change in absorbance can be attributed to the addition of the ion, leading to a decrease in overall absorbance over the light spectrum. In addition, the films with FA added appeared to have a lighter brown color compared to the dark brown color of the $MAPbI_3$ to the naked eye, an observation confirmed by the absorbance spectra. The major difference in the $MA_{0.7}FA_{0.3}PbI_3$ and $MA_{0.7}FA_{0.3}Pb(I_{0.9}Br_{0.1})_3$ perovskite films can be seen in the 700 to 800 nm range. It can be seen in Figure 11 that increasing the bromine composition of the perovskite by 15% results in a shift in the absorbance spectra slightly from around 760 nm to around 720 nm. This result is also observed in the data presented in Figure 28 as a 10% increase in the bromine content of the perovskite resulted in a noticeable shift in the absorbance spectra.

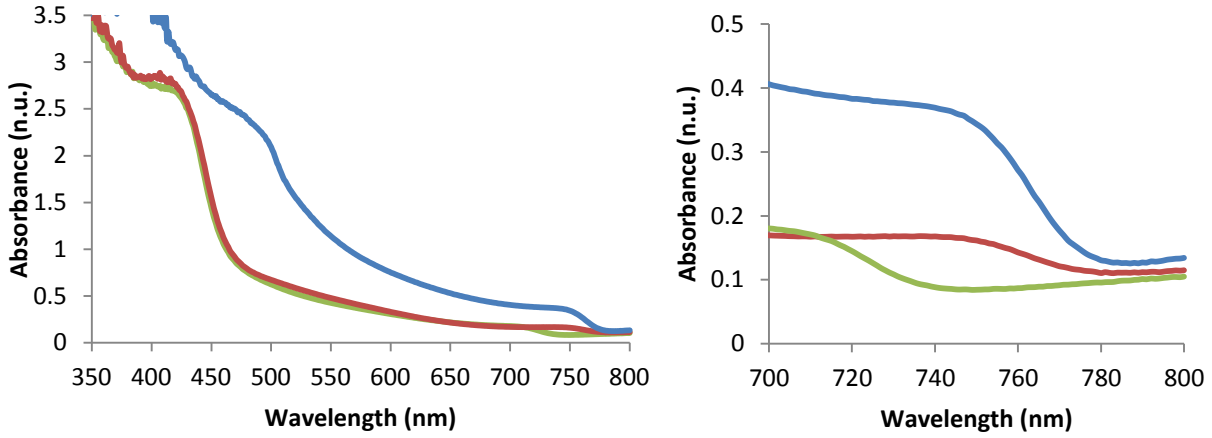

Figure 28: *Initial absorbance spectra of (blue) $MAPbI_3$, (red) $MA_{0.7}FA_{0.3}PbI_3$, and (green) $MA_{0.7}FA_{0.3}Pb(I_{0.9}Br_{0.1})_3$ perovskite films*

Under the SEM, the films for each respective recipe, shown in Figure 29, indicated that a crystalline film was formed that was consistent with literature images, as seen in Figure 30. Small pin holes can be seen in all of the images, indicating imperfections in the crystal structure, in addition to cracking along the grain boundaries. This cracking, as mentioned by Jacobsson, et al. (2016), is due to the charging effects of the electron beam of the SEM. After recording these images, zooming out reveals cracks only in the previously imaged area.

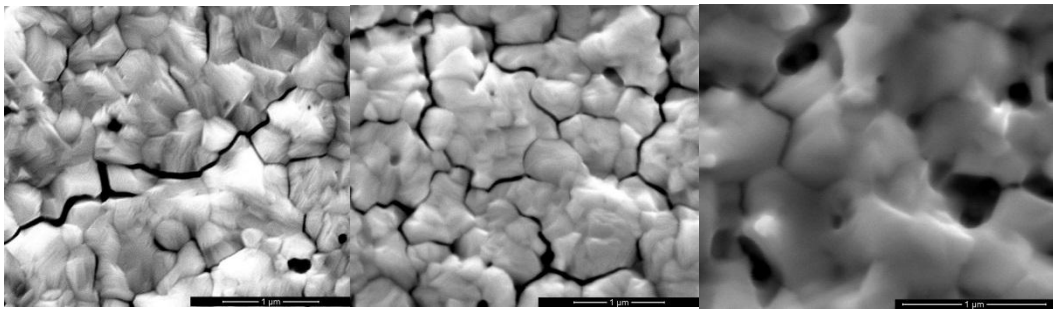

Figure 29: *(From left to right) SEM images of $MAPbI_3$, $MA_{0.7}FA_{0.3}PbI_3$, and $MA_{0.7}FA_{0.3}Pb(I_{0.9}Br_{0.1})_3$ perovskite films*

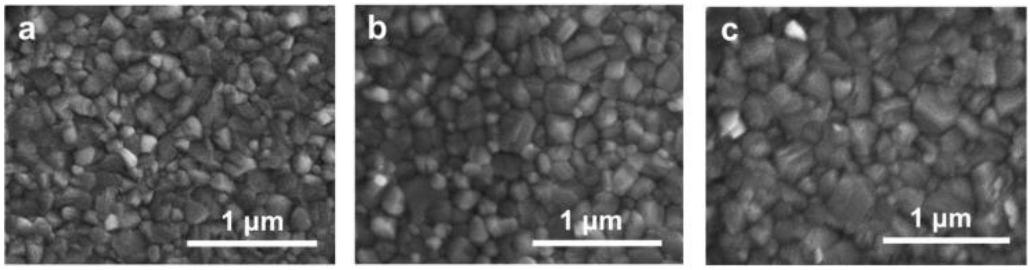

Figure 30: *SEM images of (a) $MAPbI_3$, (b) $MA_{0.7}FA_{0.3}PbI_3$, and (c) $MA_{0.7}FA_{0.3}Pb(I_{0.9}Br_{0.1})_3$ perovskite films (Yang et al., 2016)*

The experimental set-up for the *in situ* testing in this study was validated by comparing results to the results of the study completed by Yang et al. (2015). The results of the authors' 98% RH test on $MAPbI_3$ can be seen in Figure 31. The spectra collected as a part of the 85% RH test on $MAPbI_3$ can be seen in Figure 32. This graph of scans separated by 15 minutes closely matches the literature equivalent presented. The absorption characteristics are nearly identical, including the isosbestic point. This was taken as confirmation that the experimental set up worked as intended. Using the plotted spectra at 410 nm, the half-life of the film was determined to be 31 hours as seen in Figure 32.

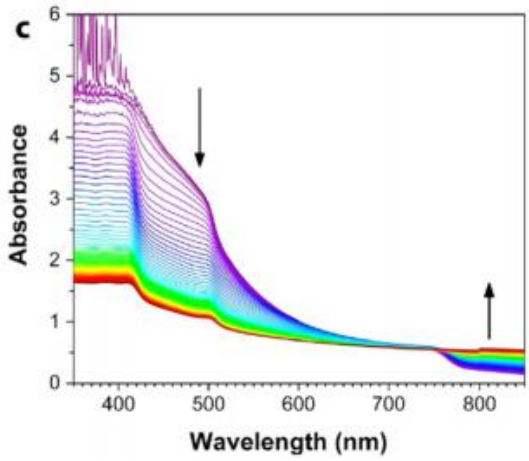

Figure 31: *Absorbance spectrum of the degradation of $MAPbI_3$ perovskite under 98% RH (Yang, et al., 2015)*

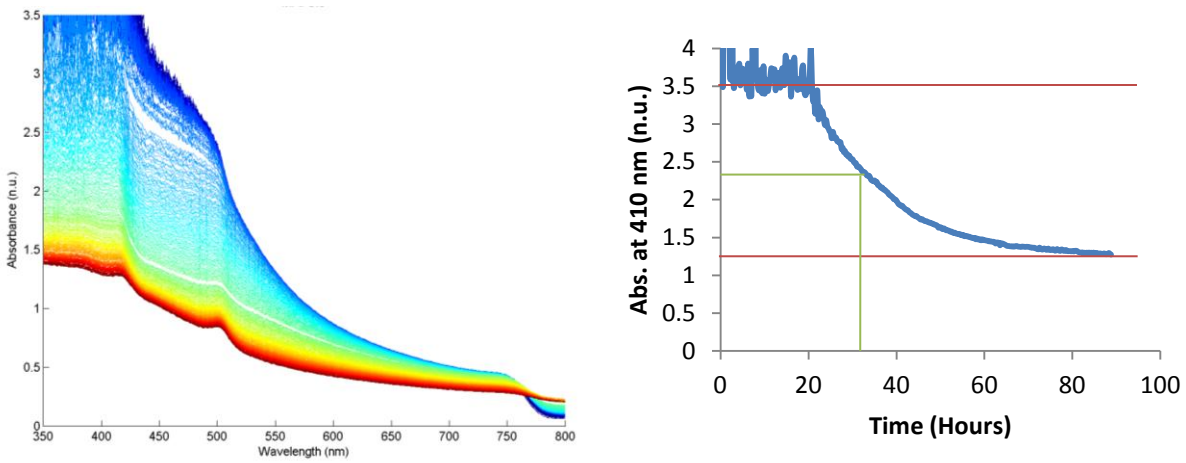

Figure 32: *Absorbance spectra, taken every 15 min., of the degradation (blue to red) of $MAPbI_3$ perovskite under 85% RH (left) and half-life determination of the film (right)*

The spatial evolution of degradation of the $MAPbI_3$ perovskite film under the 85% RH exposure can be seen in photographs shown in Figure 33. As time progresses, the dark brown perovskite degrades into the yellow lead iodide. It appears as though that the degradation starts at weak parts of the film, perhaps at the pin holes in the surface. From there, it appears to follow the grain boundaries of the crystals, seemingly hydrating the perovskite crystals. The transition from a pristine film to a degraded one is site specific, with parts of the film remaining intact for longer period than others. However, exposure to moisture ultimately causes the complete transformation of the material, as the entire film takes on the yellow color of lead iodide. This evidence of uneven spatial evolution is an important complement to the fixed-site absorbance readings. Instead of a uniform conversion to lead iodide over the entire film, the absorbance reading could vary based on which part of the film was scanned. These results are similar to observations by Yang et al. (2015), who observed a similar breakdown as seen in Figure 34.

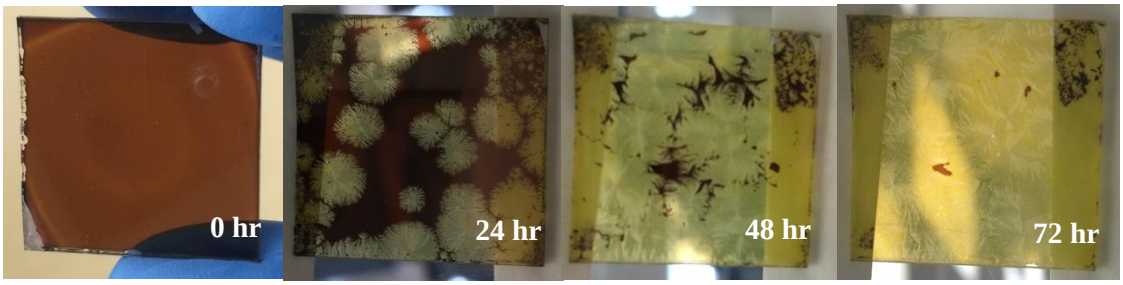

Figure 33: *$MAPbI_3$ perovskite during 85% RH exposure after 0, 24, 48, and 72 hours*

Figure 34: *$MAPbI_3$ perovskite during 98% RH exposure test (Yang, et al., 2015)*

Under the XRD, the $MAPbI_3$ perovskite exhibited the diffraction peaks that are seen in literature and detailed in Figure 5. These can be seen in Figure 35 as the initial scan with the major peak occurring at 13.52°. The additional scans shed light on the effects of increased humidity on the degradation of the films. In Figure 35, the appearance and large increase in the intensity of the lead iodide diffraction peaks indicate a breakdown of the perovskite film in all of the RH tests. Over the 2 day test period, the 30% RH exposure generated only a small lead iodide peak when compare to the 50% RH test as the perovskite peaks were diminished. However, the peak around 12° is more intense on the 85% RH EOL test film. This indicates a more complete breakdown and conversion of the film into lead iodide when the film is fully degraded.

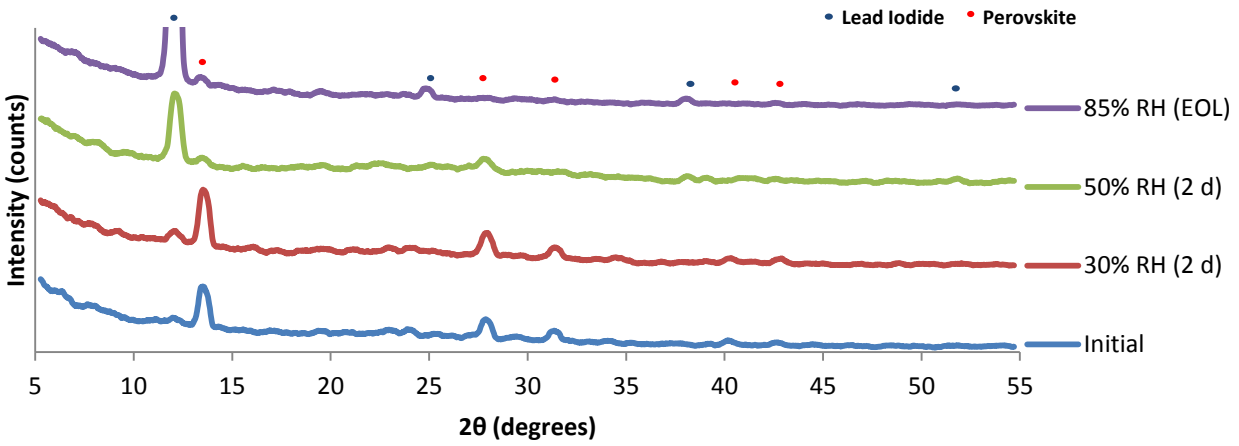

Figure 35: *XRD spectra of $MAPbI_3$ before and after 85%, 30%, and 50% RH exposure.*

In the FTIR-ATR spectra, the degradation of the N-H bond peaks is readily apparent. Although there is minimal degradation under 30% RH after 2 days, the 50% RH drastically reduced the signal intensity. It can also be seen in Figure 36 that the EOL film created under 85% RH saw a complete loss in the signal intensity, suggesting the loss of methylamine through the hydration of MAI, consistent with conversion of the perovskite film into lead iodide.

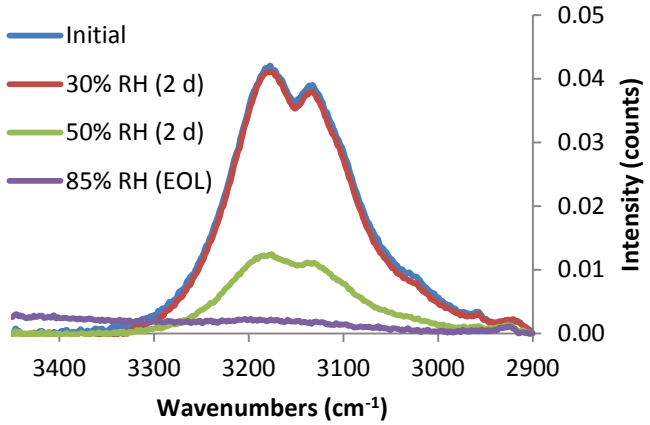

Figure 36: *FTIR-ATR spectra of $MAPbI_3$ before and after 85%, 30%, and 50% RH exposure*

The spectra of $MA_{0.7}FA_{0.3}PbI_3$ degrading under 85% RH taken every 15 minutes can be seen in Figure 37. The data indicates a rapid degradation of the film. Using the plotted spectra at 410 nm, the half-life of the film was determined to be 9 hours, as seen in Figure 37. By comparing these results to those of $MAPbI_3$, it can be observed that the addition of FA may decrease the stability of the film with respect to atmospheric moisture.

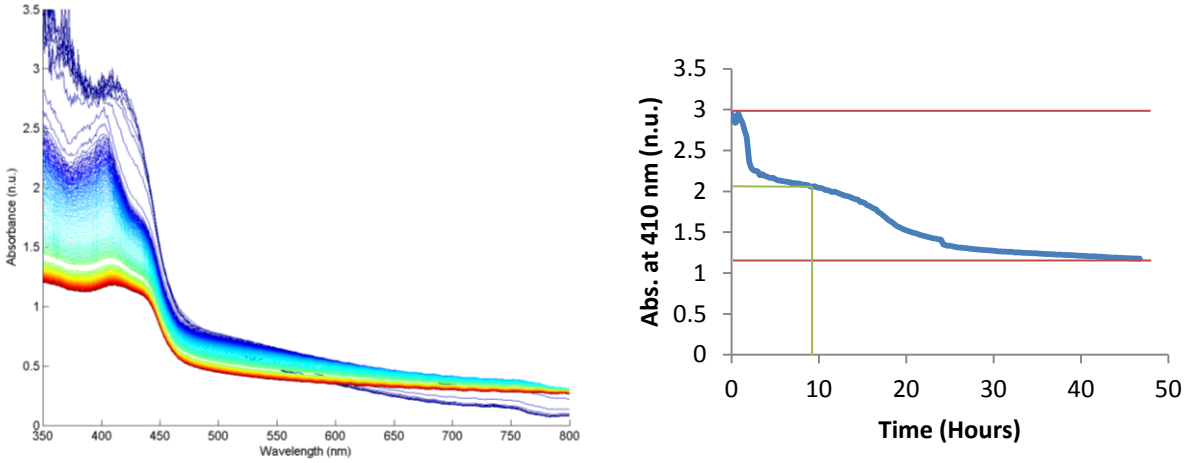

Figure 37: *Absorbance spectra, taken every 15 min., of the degradation (blue to red) of $MA_{0.7}FA_{0.3}PbI_3$ under 85% RH (left) and half-life determination of the film (right)*

The series of photographs included in Figure 38 depicts the degradation of the $MA_{0.7}FA_{0.3}PbI_3$ perovskite film under the 85% RH exposure. It can be seen that the degradation, similar to the $MAPbI_3$ film, appears to start at weak parts of the film, potentially at the grain boundaries. From there, the degradation appears to slowly spread, perhaps as the surrounding perovskite crystals are hydrated. This leads to a slow transition to the yellow color of the lead iodide. Similar to the $MAPbI_3$ film, he transition from a pristine film to a degraded is site specific, as parts of the film remain intact for longer period than others.

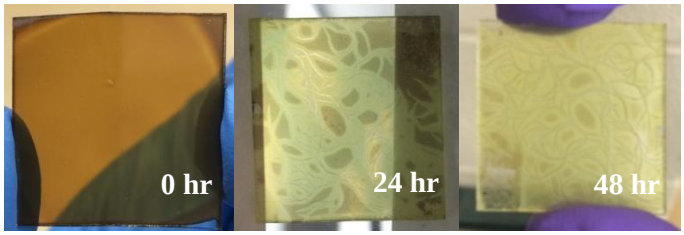

Figure 38: *$MA_{0.7}FA_{0.3}PbI_3$ perovskite during 85% RH exposure after 0, 24, and 48 hours*

In the case of the $MA_{0.7}FA_{0.3}PbI_3$ perovskite, the XRD scan, seen in Figure 39, showed a similar pattern of degradation to the $MAPbI_3$. The initial scan included diffraction peaks corresponding to the perovskite crystal structure as identified in literature with the major peak occurring at 13.48°. This shift in the diffraction peak down 0.04° from the $MAPbI_3$ peak is consistent with literature values and indicates the incorporation of the FA into the perovskite crystal structure. With humidity exposure, lead iodide peaks started to appear, although without the same intensity as the $MAPbI_3$ perovskite. No perovskite peaks remained after fully degrading the film under 85% RH. Similarly, even after 2 days of exposure to 50% RH, the perovskite diffraction peaks were non-existent. This shows how quickly the film degrades under even a moderate RH. However, after 2 days of exposure to 30% RH, the perovskite peaks remained, showing moderate stability in low RH environments.

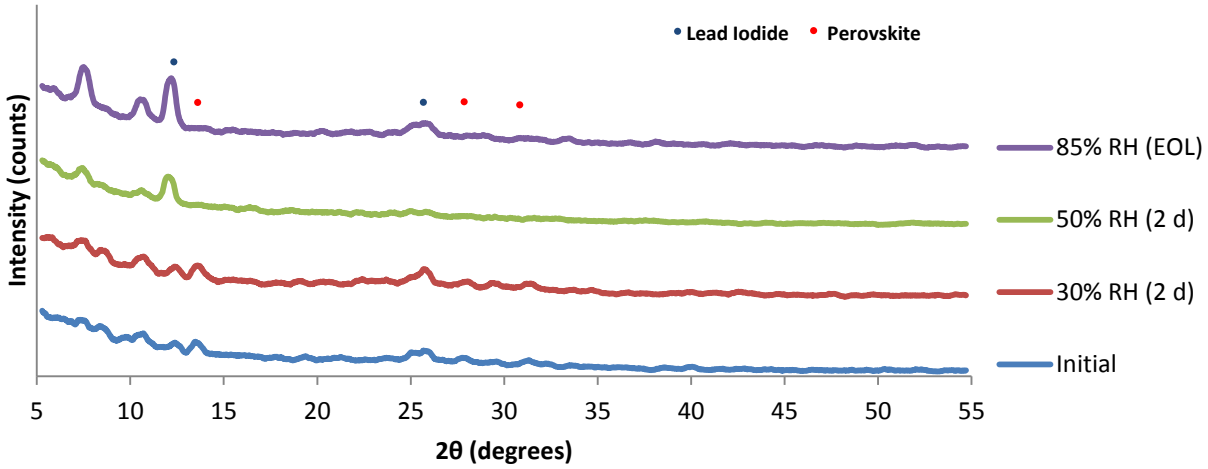

Figure 39: *XRD spectra of $MA_{0.7}FA_{0.3}PbI_3$ before and after 85%, 30%, and 50% RH exposure*

The FTIR-ATR spectra for $MA_{0.7}FA_{0.3}PbI_3$, seen in Figure 40, show a number of interesting features of the films. First, two additional peaks at 3275 cm^{-1} and 3325 cm^{-1} appeared in the spectra. In addition, the peak at 3175 cm^{-1} appeared to be half as intense as the corresponding peak in the $MAPbI_3$ spectra. To understand these new additions, FTIR-ATR spectra were taken for MAI and FAI, as seen in Figure 41. In this plot, a peak associated with FAI is present at 3325 cm^{-1} where the MAI spectrum has no intensity readings. With this information, it can be shown that there is a FA presence in the films. After exposure to increased humidity conditions, the intensity of the N-H stretch is diminished, suggesting the loss of methylamine and formamidine through the hydration of MAI and FAI respectively. It can also be seen that the intensity of the N-H stretch tends to be diminished more rapidly than the additional peaks associated with the FAI. This remaining signal intensity suggests that the methylamine leaves the perovskite structure more rapidly than formamidine.

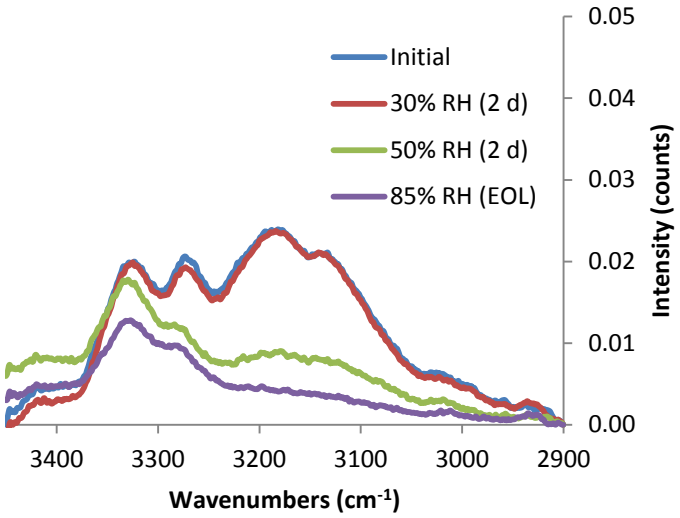

Figure 40: *FTIR-ATR spectra of $MA_{0.7}FA_{0.3}PbI_3$ perovskite before and after 85%, 30%, and 50% RH exposure*

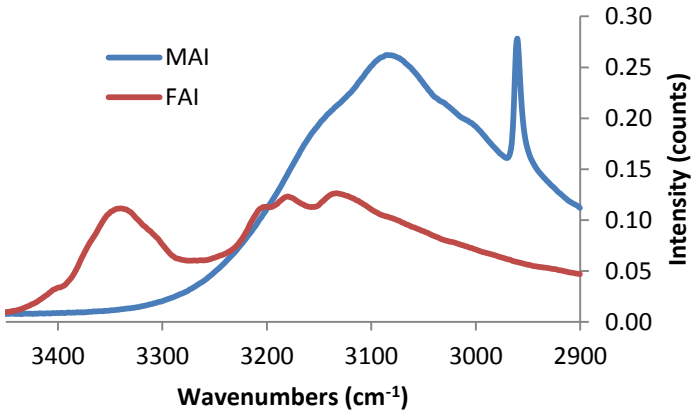

Figure 41: *FTIR-ATR spectra of MAI and FAI*

The spectra collected during the 85% RH test on $MA_{0.7}FA_{0.3}Pb(I_{0.9}Br_{0.1})_3$ can be seen in Figure 42. This series of scans, each separated by 1 hour, shows a slow initial degradation of the film, followed by a faster degradation before slowing down again. Using the plotted spectra at 410 nm, the half-life of the film was determined to be 15 hours. By comparing Figure 42 to

Figure 37, it can be observed that although nuances in the degradation spectra, like the dip around 350 nm, are the same in both films, the addition of the bromine ion appeared to have slowed down the initial degradation process.

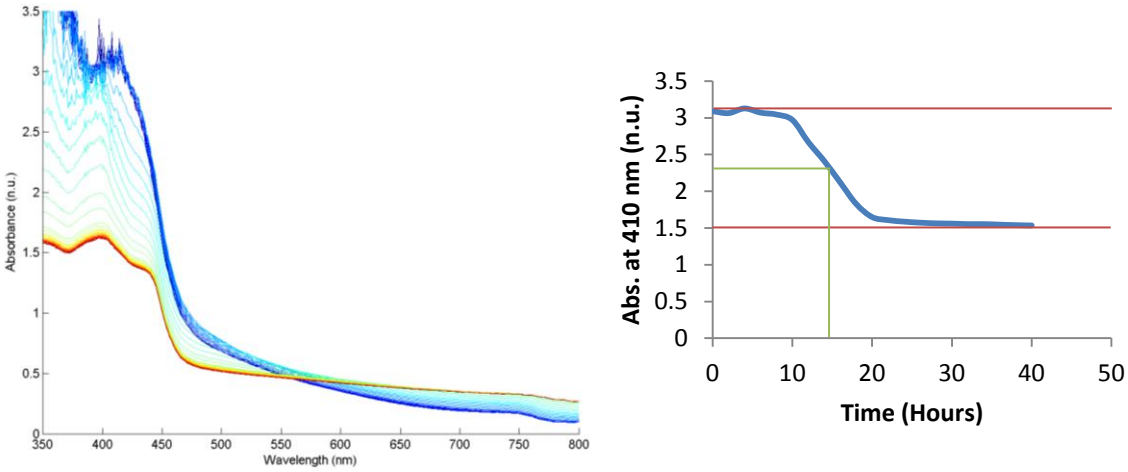

Figure 42: *Absorbance spectra, taken every hour, of the degradation (blue to red) of* $MA_{0.7}FA_{0.3}Pb(I_{0.9}Br_{0.1})_3$ *under 85% RH (left) and half-life determination of the film (right)*

The series of pictures included in Figure 43 depicts the degradation of the $MA_{0.7}FA_{0.3}Pb(I_{0.9}Br_{0.1})_3$ perovskite film under the 85% RH exposure. The film degradation goes from left to right, as the brown perovskite degrades into the yellow lead iodide. The pictures were taken during the experiment after 0, 12, and 36 hours. It can be seen that the degradation, unlike the other films, appears to uniform over the entire surface. Instead of seeing degradation at the grain boundaries and pinholes in the film, a cloudiness came over the film as it transitioned from brown to yellow. This uniformity could be due to the improved crystallinity of the films due to the bromine ion addition to the crystal structure.

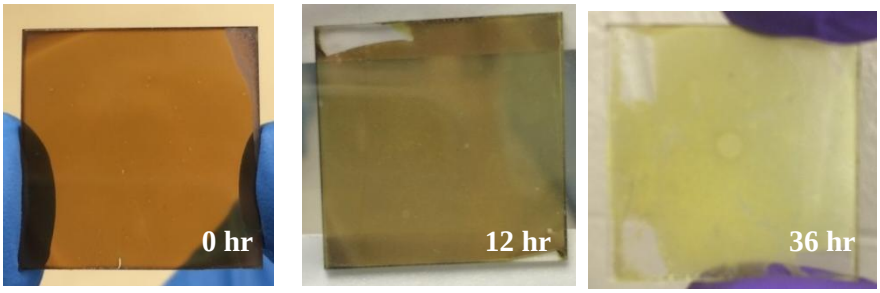

Figure 43: $MA_{0.7}FA_{0.3}Pb(I_{0.9}Br_{0.1})_3$ *during 85% RH exposure after 0, 12, and 36 hours*

The initial scan of the $MA_{0.7}FA_{0.3}Pb(I_{0.9}Br_{0.1})_3$ perovskite showed diffraction peaks corresponding to the perovskite crystal structure as identified in literature with the major peak occurring at 13.54°. This shift in the diffraction peak up 0.06° from the $MA_{0.7}FA_{0.3}PbI_3$ peak is consistent with literature values and indicates the incorporation of the Br^- ions into the perovskite crystal structure. As seen with the other perovskite films, humidity exposure caused the appearance of lead iodide peaks, although without the same intensity as the $MAPbI_3$ perovskite. In addition, the initial perovskite diffraction peaks for the $MA_{0.7}FA_{0.3}Pb(I_{0.9}Br_{0.1})_3$ were not as defined as the other films, and lead iodide peaks were present in the initial scan, suggesting imperfect initial formation of the film. Under 30% RH, the perovskite diffraction peaks remain intact, but increased humidity causes them to disappear. Under 50% RH exposure, the perovskite peak is replaced by a larger lead iodide peak. Similarly, after complete degradation of the film under 85% RH, no perovskite peaks remained and additional lead iodide peaks appeared in the spectra. These features can be seen in Figure 44.

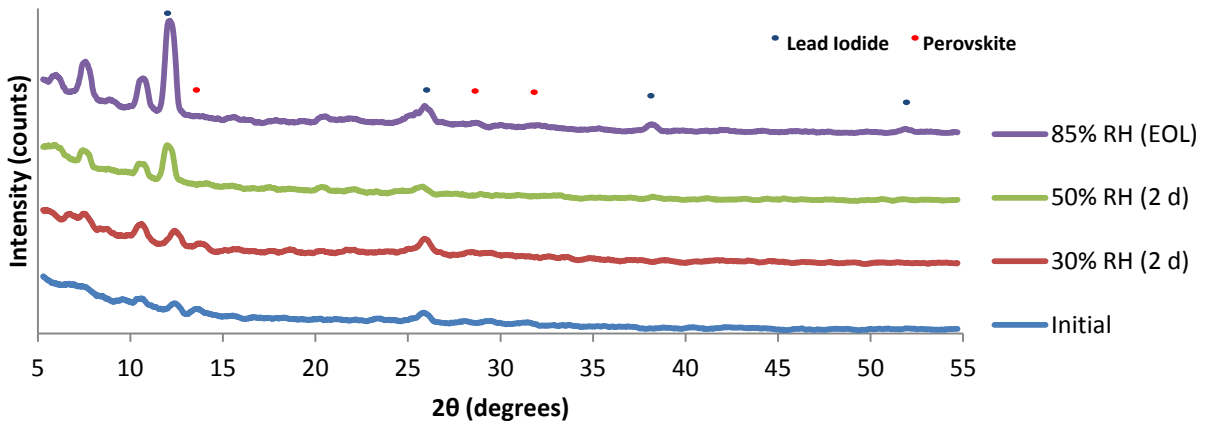

Figure 44: *XRD spectra of $MA_{0.7}FA_{0.3}Pb(I_{0.9}Br_{0.1})_3$ before and after 85%, 30%, and 50% RH exposure*

The FTIR-ATR spectra for $MA_{0.7}FA_{0.3}Pb(I_{0.9}Br_{0.1})_3$ can be seen in Figure 45. Compared to the Figure 40, the same general peaks are present and with similar intensities. However, the peak at 3275 cm^{-1} is less intense than the one seen in Figure 40. This change in peak intensity could indicate an addition of bromine into the perovskite film. In addition, under high humidity, the intensities of the N-H peaks tend to decrease more rapidly than the additional FAI associated peaks, as seen in the $MA_{0.7}FA_{0.3}PbI_3$ film.

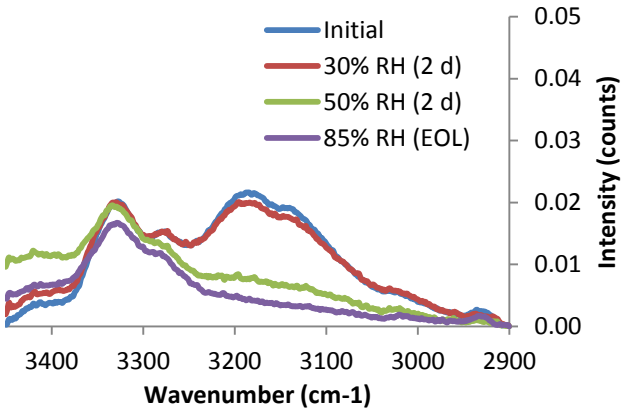

Figure 45: *FTIR-ATR spectra of $MA_{0.7}FA_{0.3}Pb(I_{0.9}Br_{0.1})_3$ before and after 85%, 30%, and 50% RH exposure*

Conclusions

The purpose of this project was to determine how perovskite films with varying ion compositions react in controlled atmospheric conditions. Through *in situ* testing under high humidity conditions and subsequent lower humidity testing, an in depth picture of the degradation pathway of three different perovskite films was formed. The effect of formamidinium and bromine ion incorporation into perovskite crystals were examined through the fabrication of $MA_{0.7}FA_{0.3}PbI_3$ and $MA_{0.7}FA_{0.3}Pb(I_{0.9}Br_{0.1})_3$ films and comparing them to $MAPbI_3$ perovskite films.

It was shown through every test on every perovskite that humidity had a large and detrimental effect on perovskite films. The degradation pathways may vary, but the final results always indicated a breakdown of the perovskite crystal structure, resulting in the formation of lead iodide. Results of this breakdown were seen using a number of different characterization techniques.

Through the use of the UV-vis, the absorption spectra of each film could be analyzed over time. It can be seen that each spectrum continually shifts from its initial shape to its final shape smoothly. This transition suggests a simple transformation from the perovskite crystals to lead iodide. If transformations involving multiple products at different rates were occurring during the reaction, more complex shifts and features would be present in the spectra over the degradation time period. In addition, the absorbance spectra showed the initial light absorbing characteristics of each film and gave indications of the films stability over time. For the $MA_{0.7}FA_{0.3}PbI_3$ and $MA_{0.7}FA_{0.3}Pb(I_{0.9}Br_{0.1})_3$ films, new degradation rates were observed, showing a faster breakdown of the film with the use of FA ions when compared to $MAPbI_3$. However, the incorporation of bromine slowed the degradation process, recovering some of the

stability that was lost. This was concluded as the half-lives for the $MAPbI_3$, $MA_{0.7}FA_{0.3}PbI_3$, and $MA_{0.7}FA_{0.3}Pb(I_{0.9}Br_{0.1})_3$ films were 31 hours, 9 hours, and 15 hours respectively. Pairing this data with visual and SEM data provides a more holistic picture of the degradation. The spectrophotometer measures the absorbance in a select area of the film. However, it was seen that the location of this sampling point can influence the data over time. For the perovskite films that did not contain bromide ions, the degradation was localized compared to the uniform degradation of the $MA_{0.7}FA_{0.3}Pb(I_{0.9}Br_{0.1})_3$ film. The hypothesis that this originates at imperfections in the films is supported by SEM observations of pinholes in the films.

Using the XRD and FTIR-ATR, the degradation could be observed from a chemical structure standpoint. The XRD scans gave an indication of the crystal structures present in the films and their accompanying intensities. With this, it was clear that the $MAPbI_3$ was the best formed perovskite as the peaks shown were confirmed through literature as perovskite peaks and that not lead iodide was initially present. The XRD spectra for the other films indicated imperfections, with peaks for lead iodide in the initial sample and less intense perovskite peaks. However, the XRD scans did confirm the incorporation of the additional ions into the crystal structure through slight peak shifts. Similarly, the FTIR-ATR data indicated this incorporation through the addition of bonding peaks associated with FAI when the $MA_{0.7}FA_{0.3}PbI_3$ and $MA_{0.7}FA_{0.3}Pb(I_{0.9}Br_{0.1})_3$ films were examined. In addition, the intensity of the N-H bonding peaks dropped by almost half when compared to the $MAPbI_3$ film. This is further indication in a shift of bonding as both MA and FA ions are utilized in the perovskite structure.

Overall, by combining all of these measurements, a complete picture of the degradation of each of these perovskite films was formed. The addition of FA ions into the perovskite appeared to have adverse effects on the stability of the film from a humidity standpoint. On the

contrary, the addition of bromine ions appeared to increase the stability of the films versus humidity.

Future Testing

Future work will require refined procedures for the fabrication of $MA_{0.7}FA_{0.3}PbI_3$ and $MA_{0.7}FA_{0.3}Pb(I_{0.9}Br_{0.1})_3$ films. In order to create pristine films of complete perovskite crystals, controlled environments and pure chemicals are necessary. However, this comes with an associated cost increase. With pristine films, testing through the incorporation of the films into solar cell devices would provide an understanding of the films potential PCEs and further applicability. In that regard, humidity testing on whole solar cell devices would provide researchers a glimpse into the stability of the devices in real world environments.

Testing of alternative materials has started in the attempt to make perovskites more stable in humid atmospheres. In a study completed by Smith et al. (2014), perovskites in the form $(PEA)_2(MA)_2(Pb_3I_{10})$ where PEA is $C_6H_5(CH_2)_2NH_3^+$ were fabricated and compared to $MAPbI_3$ perovskite films and cells. Through XRD measurements, as seen in Figure 46, it was clear that this new material offered superior stability in a 52% RH atmosphere. While the $MAPbI_3$ film was degraded to PbI_2, the PEA perovskite remained unaffected. Although the PEA films produced solar cells with a PCE of 4.73%, their moisture stability remains as an improvement over traditional perovskite films. The authors also remarked that hydrophobic fluorocarbons could increase moisture stability. (Smith et al., 2014)

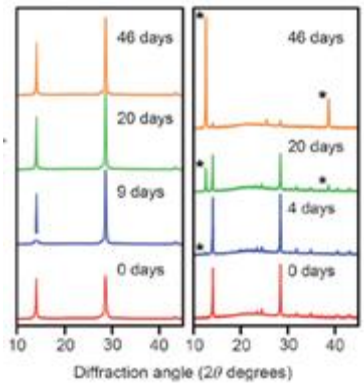

Figure 46: *XRD scans showing the degradation of* $(PEA)_2(MA)_2(Pb_3I_{10})$ *(left) and* $MAPbI_3$ *(right) perovskites under 52% RH (Smith, et al., 2014)*

In addition, it was noted that by simply covering the perovskite films would help deter degradation due to atmospheric moisture. This simple concept was observed during the study and picture in Figure 47 illustrates the boundary of the covered and uncovered areas.

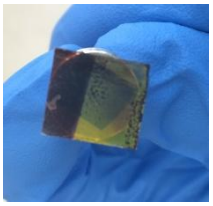

Figure 47: *The effects of partially covering a perovskite film during degradation*

Further testing utilizing different ions and combinations of ions into the perovskite structure could lead a more diverse understanding of the effects of moisture on perovskite films. As the eventual goal for perovskite solar cells is to replace or be used in tandem with silicon solar cells, testing and manufacturing films that can withstand environmental conditions will become more important than simply creating the most efficient solar cell possible. A balance of

efficiency and stability must be reached in order to find the best possible perovskite solar cell for general application. In a world committed to the environment, the additional testing of non-lead based films could help expand the potential application of this technology and make it more widely accepted. In addition, finding new and innovative ways of applying the technology, such as in building applications as an energy generating “stained glass”, could expand the market and lead to the mass usage of ion tuned perovskite solar cells.

Works Cited

Ali, N., A. Hussain, R. Ahmed, M.K. Wang, C. Zhao, B. Ul Haq, and Y.Q. Fu. "Advances in Nanostructured Thin Film Materials for Solar Cell Applications." *Renewable and Sustainable Energy Reviews* 59 (2016): 726-37.

Bag, Monojit, Lawrence A. Renna, Ramesh Y. Adhikari, Supravat Karak, Feng Liu, Paul M. Lahti, Thomas P. Russell, Mark T. Tuominen, and D. Venkataraman. "Kinetics of Ion Transport in Perovskite Active Layers and Its Implications for Active Layer Stability." *Journal of the American Chemical Society* 137.40 (2015): 13130-3137.

Berdiyorov, G.R., F. El-Mellouhi, M.E. Madjet, F.H. Alharbi, F.M. Peeters, and S. Kais. "Effect of Halide-mixing on the Electronic Transport Properties of Organometallic Perovskites." *Solar Energy Materials and Solar Cells* 148 (2016): 2-10.

Christians, Jeffrey A., Pierre A. Miranda Herrera, and Prashant V. Kamat. "Transformation of the Excited State and Photovoltaic Efficiency of $CH_3NH_3PbI_3$ Perovskite upon Controlled Exposure to Humidified Air." *Journal of the American Chemical Society* 137.4 (2015): 1530-538.

Correa Baena, Juan Pablo, Ludmilla Steier, Wolfgang Tress, Michael Saliba, Stefanie Neutzner, Taisuke Matsui, Fabrizio Giordano, T. Jesper Jacobsson, Ajay Ram Srimath Kandada, Shaik M. Zakeeruddin, Annamaria Petrozza, Antonio Abate, Mohammad Khaja Nazeeruddin, Michael Grätzel, and Anders Hagfeldt. "Highly Efficient Planar Perovskite Solar Cells through Band Alignment Engineering." *Energy Environ. Sci.* 8.10 (2015): 2928-934.

Cui, Dong, Zhou Yang, Dong Yang, Xiaodong Ren, Yucheng Liu, Qingbo Wei, Haibo Fan, Jinghui Zeng, and Shengzhong (Frank) Liu. "Color-Tuned Perovskite Films Prepared for Efficient Solar Cell Applications." *The Journal of Physical Chemistry C* 120.1 (2016): 42-47.

Docampo, Pablo, James M. Ball, Mariam Darwich, Giles E. Eperon, and Henry J. Snaith. "Efficient Organometal Trihalide Perovskite Planar-heterojunction Solar Cells on Flexible Polymer Substrates." *Nature Communications* 4 (2013)

Gao, Qianqian, Songwang Yang, Lei Lei, Shude Zhang, Qipeng Cao, Junjie Xie, Jiaqing Li, and Yan Liu. "An Effective TiO_2 Blocking Layer for Perovskite Solar Cells with Enhanced Performance." *Chemistry Letters* 44.5 (2015): 624-26.

Gonzalez-Pedro, Victoria, Emilio J. Juarez-Perez, Waode-Sukmawati Arsyad, Eva M. Barea, Francisco Fabregat-Santiago, Ivan Mora-Sero, and Juan Bisquert. "General Working Principles of $CH_3NH_3PbX_3$ Perovskite Solar Cells." *Nano Letters* 14.2 (2014): 888-93.

Hodes, G. "Perovskite-Based Solar Cells." *Science* 342.6156 (2013): 317-18.

Jacobsson, T. Jesper, Juan-Pablo Correa-Baena, Meysam Pazoki, Michael Saliba, Kurt Schenk, Michael Grätzel, and Anders Hagfeldt. "Exploration of the Compositional Space for Mixed Lead Halogen Perovskites for High Efficiency Solar Cells." *Energy Environ. Sci.* 9.5 (2016): 1706-724.

Jeon, Nam Joong, Jun Hong Noh, Young Chan Kim, Woon Seok Yang, Seungchan Ryu, and Sang Il Seok. "Solvent Engineering for High-performance Inorganic–organic Hybrid Perovskite Solar Cells." *Nature Materials* 13.9 (2014): 897-903.

Ke, Weijun, Guojia Fang, Jing Wang, Pingli Qin, Hong Tao, Hongwei Lei, Qin Liu, Xin Dai, and Xingzhong Zhao. "Perovskite Solar Cell with an Efficient TiO_2 Compact Film." *ACS Applied Materials & Interfaces* 6.18 (2014): 15959-5965.

Leguy, Aurélien M. A., Yinghong Hu, Mariano Campoy-Quiles, M. Isabel Alonso, Oliver J. Weber, Pooya Azarhoosh, Mark Van Schilfgaarde, Mark T. Weller, Thomas Bein, Jenny Nelson, Pablo Docampo, and Piers R. F. Barnes. "Reversible Hydration of $CH_3NH_3PbI_3$ in Films, Single Crystals, and Solar Cells." *Chemistry of Materials* 27.9 (2015): 3397-407.

Pellet, Norman, Peng Gao, Giuliano Gregori, Tae-Youl Yang, Mohammad K. Nazeeruddin, Joachim Maier, and Michael Grätzel. "Mixed-Organic-Cation Perovskite Photovoltaics for Enhanced Solar-Light Harvesting." *Angew. Chem*. 126.12 (2014): 3215-221.

Ruess, Raffael, Felix Benfer, Felix Boecher, Martina Stumpp, and Derck Schlettwein. "Stabilization of Organic-Inorganic Perovskite Layers by Partial Substitution of Iodide by Bromide in Methylammonium Lead Iodide." *Chem Phys Chem* (2016)

Smith, Ian C., Eric T. Hoke, Diego Solis-Ibarra, Michael D. Mcgehee, and Hemamala I. Karunadasa. "A Layered Hybrid Perovskite Solar-Cell Absorber with Enhanced Moisture Stability." *Angewandte Chemie International Edition* 53.42 (2014): 11232-1235.

Supasai, T., N. Rujisamphan, K. Ullrich, A. Chemseddine, and Th. Dittrich. "Formation of a Passivating CH3NH3PbI3/PbI2 Interface during Moderate Heating of $CH_3NH_3PbI_3$ Layers." *Applied Physics Letters* 103.18 (2013): 183906.

Tong, Chuan-Jia, Wei Geng, Zhen-Kun Tang, Chi-Yung Yam, Xiao-Li Fan, Jiang Liu, Woon-Ming Lau, and Li-Min Liu. "Uncovering the Veil of the Degradation in Perovskite

$CH_3NH_3PbI_3$ upon Humidity Exposure: A First-Principles Study." *The Journal of Physical Chemistry Letters* 6.16 (2015): 3289-295.

Weber, Dieter. "$CH_3NH_3PbX_3$, Ein Pb(II)-System Mit Kubischer Perowskitstruktur / $CH_3NH_3PbX_3$, a Pb(II)-System with Cubic Perovskite Structure." *Zeitschrift Für Naturforschung B* 33.12 (1978)

Wozny, Sarah, Mengjin Yang, Alexandre M. Nardes, Candy C. Mercado, Suzanne Ferrere, Matthew O. Reese, Weilie Zhou, and Kai Zhu. "Controlled Humidity Study on the Formation of Higher Efficiency Formamidinium Lead Triiodide-Based Solar Cells." *Chemistry of Materials* 27.13 (2015): 4814-820.

Yang, Jinli, Braden D. Siempelkamp, Dianyi Liu, and Timothy L. Kelly. "Investigation of $CH_3NH_3PbI_3$ Degradation Rates and Mechanisms in Controlled Humidity Environments Using in Situ Techniques." *ACS Nano* 9.2 (2015): 1955-963.

Yang, Zhibin, Chu-Chen Chueh, Po-Wei Liang, Michael Crump, Francis Lin, Zonglong Zhu, and Alex K.-Y. Jen. "Effects of Formamidinium and Bromide Ion Substitution in Methylammonium Lead Triiodide toward High-performance Perovskite Solar Cells." *Nano Energy* 22 (2016): 328-37.

Wang, Dian, Matthew Wright, Naveen Kumar Elumalai, and Ashraf Uddin. "Stability of Perovskite Solar Cells." *Solar Energy Materials and Solar Cells* 147 (2016): 255-75.